



A modified transfer matrix method for the coupling lateral and torsional vibrations of symmetric rotor-bearing systems

Sheng-Chung Hsieh^a, Juhn-Horng Chen^b, An-Chen Lee^{a,*}

^a*Department of Mechanical Engineering, National Chiao Tung University, 1001 Ta Hsueh Road, Hsinchu 30049, Taiwan, ROC*

^b*Department of Mechanical Engineering, Chung Hua University, Taiwan, ROC*

Received 27 January 2004; received in revised form 9 August 2004; accepted 8 February 2005

Available online 28 April 2005

Abstract

This study develops a modified transfer matrix method for analyzing the coupling lateral and torsional vibrations of the symmetric rotor-bearing system with an external torque. Euler's angles are used to describe the orientations of the shaft element and disk. Additionally, to enhance accuracy, the symmetric rotating shaft is modeled by the Timoshenko beam and considered using a continuous-system concept rather than the conventional "lumped system" concept. Moreover, the harmonic balance method is adopted in this approach to determine the steady-state responses comprising the synchronous and superharmonic whirals. According to our analysis, when the unbalance force and the torque with $n \times$ frequency of the rotating speed excite the system simultaneously, the $(n + 1) \times$ and $(n - 1) \times$ whirals appear along with the synchronous whirl. Finally, several numerical examples are presented to demonstrate the applicability of this approach.

© 2005 Elsevier Ltd. All rights reserved.

1. Introduction

Rotor dynamics plays an important role in many engineering fields, such as gas turbine, steam turbine, reciprocating and centrifugal compressors, the spindle of machine tools, and so on. Owing to the growing demands for high power, high speed, and light weight of the rotor-bearing

*Corresponding author. Tel.: + 886 3 5728513; fax: 886 3 5725372.

E-mail address: aclee@cc.nctu.edu.tw (An-Chen Lee).

Nomenclature	
E, G	Young's modulus and shear modulus
A, ρ	cross-sectional area and density of the shaft
I^s, I_p^s	transverse and polar area moment of inertia of the shaft
I^d, I_p^d	transverse and polar mass moment of inertia of the disk
L	length of the shaft element
k_s	Timoshenko's shear coefficient
e	eccentricity
m	mass
K_{xx}, K_{yy}	direct axial stiffness of the bearing
K_{xy}, K_{yx}	cross-axial stiffness of the bearing
$K_{\theta xx}, K_{\theta yy}$	direct bending stiffness of the bearing
$K_{\theta xy}, K_{\theta yx}$	cross-bending stiffness of the bearing
K_ϕ	torsional stiffness of the bearing
C_{xx}, C_{yy}	direct axial damping of the bearing
C_{xy}, C_{yx}	cross-axial damping of the bearing
$C_{\theta xx}, C_{\theta yy}$	direct bending damping of the bearing
$C_{\theta xy}, C_{\theta yx}$	cross-bending damping of the bearing
C_ϕ	torsional damping of the bearing
Ω	rotating speed
t	time
M	bending moment in fixed frame
V	shear force in fixed frame
T	axial torque
T^b	torque due to bearing
x, y	deflections of the geometric center in X and Y directions
x_c, y_c	deflections of the mass center in X and Y directions
θ	angular displacements
γ	shear deformation angles
φ	angle of twist
\mathbf{S}	state variable vector
\mathbf{X}	general displacement state variable vector
\mathbf{F}	general force state variable vector
$\mathbf{X}(Z)$	mode function vector of general displacement
$\mathbf{F}(Z)$	mode function vector of general force
$[T]$	transfer matrix
$[U]$	overall transfer matrix
E_k, E_p	kinetic energy and potential energy
W	work
w	weight
XYZ	fixed frame
UVW	rotating frame coincident with principal axes of rotating element
ϕ, θ, ψ	Euler's angles with rotating order in rank
Φ	spin angle of the rotating element about the axis W
Subscript	
c, s	associated to cosine, sine terms
x, y	components in X, Y directions
u, v	components in U, V directions
$\{\bullet\}, \{\cdot\}$	to be referred to as derivatives with respect to time and coordinate
Superscript	
R, L	right, left
s, d, b	superscript for shaft element, disk and bearing
h, p	homogeneous solution, particular solution

system, computations of critical speeds and steady-state response at synchronous and subcritical resonances become essential for system design, identification, diagnosis, and control.

Currently, the finite element and transfer matrix approaches are becoming two of the most prevalent methods for analyzing rotor-bearing systems. While the finite element method (FEM) formulates rotor-bearing systems by second-order differential equations directly utilized for control design and estimation, the transfer matrix method (TMM) solves dynamic problems in the

frequency domain. The TMM utilizes a marching procedure, starting with the boundary conditions at one side of the system, and successively marching along the structure to the other side of the system. The satisfaction of the boundary conditions at all boundary points provides the basis for solution location. The state of the rotor system at a specific point is transferred between successive points through transfer matrices. This method is particularly suitable for “chainlinked” structures such as rotor systems. The primary advantage of the TMM is that it does not require the storage and manipulation of large system arrays [1].

The application of finite element models to rotor dynamics has been highly successful. Numerous finite element procedures have attempted to generalize and improve the work of Ruhl and Booker [2]. Nelson and McVaugh [3] employed a finite element model to formulate the dynamic equation of a linear rotor system and determine the stability and steady-state responses. Moreover, Nelson [4] and Özgüven and Özkan [5] further improved the finite element model by including the effects of rotary inertia, gyroscopic moments, shear deformation and internal damping.

Genta [6] proposed a scheme for investigating the parametric vibration and instability of an asymmetric rotor-bearing system via FEM without giving the general formulation of the motion equation. Genta thus failed to investigate the effects of asymmetry on the motion of rotor-bearing systems. The effects of deviatoric stiffness of shaft and bearing owing to asymmetry on steady-state responses was investigated by Kang et al. [7] and transient responses under acceleration was investigated by Lee et al. [8].

The TMM was first proposed by Prohl [9]. Subsequently, the effects of damping and stiffness of the fluid film bearing were included by Koenig [10], Guenther and Lovejoy [11]. Lund [12] achieved significant advances in the TMM by considering the effects of gyroscopic, internal friction and aerodynamic cross-coupling forces. Bansal and Kirk [13] applied the TMM in modal analysis for calculating the damped natural frequencies and examining the stability of flexible rotors mounted on flexible bearing supports. Lund [14] presented a scheme for estimating the sensitivity of the critical speeds of a rotor to change the design factors. The use of TMM on the rotors being exposed to a constant axial force and torque was considered by Yim et al. [15]. In the above works, the shaft is modeled using a lumped-system sense to relate the state variables of the two ends of the segment via transfer matrix. Because the lumped mass is concentrated at each end of the section, the shaft must be divided into numerous sections to yield accurate results. Consequently, considerable computing time is required.

Lund and Orcutt [16] constructed the shaft transfer matrix in a continuous-system sense analytically and examined the unbalance vibrations experimentally. Furthermore, Inagaki et al. [17] devised a TMM scheme for determining the steady-state response of asymmetric rotor-bearing systems by considering only the effect of transverse inertia, while ignoring the effects of rotary inertia and gyroscopic moment. However, their study only considered a single harmonic component for the synchronous whirl. Additionally, David et al. [18] showed that the harmonic balance technique incorporating the TMM can be applied to analyze parametric systems. Moreover, Lee et al. [19] improved the TMM of the continuous-systems sense to fit the synchronous elliptical orbits of the linear rotor-bearing systems by doubling the number of state variables to 16. Their study also considered the rotary inertia, gyroscopic and transverse shear effects. Furthermore, the utilization of TMM for continuous systems was extended to the unbalancing shaft [20] and asymmetric rotors [21]. All of the above studies assumed that the

rotating shaft in the axial direction is rigid. However, the values of the transverse amplitudes calculated based on this assumption may differ markedly from the actual values.

Regarding the torsional analysis using the TMM, Pestel and Leckie [22] provided a thorough reference for applying the transfer matrix to determine the natural frequencies and mode shape for torsional systems. Moreover, Pilkey and Chang [23] presented a generalized method for applying the boundary conditions to a torsional transfer matrix model that is useful in developing an algorithm for accomplishing the desired analysis. Sankar [24] presented one multi-shaft torsional transfer matrix approach. This method built the transfer matrix for each branch separately, applied compatibility relations at the junction, and then used the boundary conditions to obtain the characteristic determinant of the system. Finally, Rao [25] employed the TMM to analyze the free vibration, transient response, critical speed, and instability of the torsional rotor system.

Schwibinger and Nordmann [26] examined the influence of torsional–lateral coupling on the stability behavior of a simple geared system supported by oil film bearings. Schwibinger and Nordmann found that the classical eigenvalue analysis ignoring the coupling of torsional and lateral vibrations in gears might cause serious errors in the stability prediction, such as the critical speeds and natural modes. Qin and Mao [27] developed a new finite element model to analyze the torsional–flexural characteristics of the rotor system. Additionally, Rao et al. [28] investigated the lateral transient response of geared rotors raised by torsional excitation. Rao et al. concluded that even if the critical speed of the rotor did not approach the running speed, the lateral response at a multiple of the spin speed and the torsional response were very large, and the influence of incremental bending stiffness because of axial torque was insignificant. Mohiuddin and Khulief [29] presented a reduced modal form of the rotor-bearing system to find the transient responses owing to different excitations using the FEM. Al-Bedoor [30] presented a dynamic model for a typical elastic blade attached to a disk mounted on a shaft which was flexible in the torsional direction. The resulting model and simulation results exhibited strong dependence and energetic interaction between the shaft torsional deformations and the blade bending deformations. Additionally, Al-Bedoor [31] presented a model for interpreting the coupled torsional and lateral transient vibrations of the simple Jeffcott rotor. His analysis demonstrated the existence of inertial coupling and nonlinear interaction between the torsional and lateral vibrations. Lee [32] formulated the coupled equations of motion in a lateral bending–torsion for an unbalanced disk of the simple Jeffcott rotor for analyzing the instabilities.

This work develops a modified TMM for the coupling lateral and torsional vibrations of symmetric rotor-bearing systems. Euler's angles are used to describe the orientations of the shaft elements and disks. First, Hamilton's Principle and Newton's second law are used to derive the motion equations of the flexible shaft, rigid disks, and linear bearings with respect to the fixed coordinate, and second, the transfer matrices of the elements are established using the harmonic balance method. Third, the state variables of the element matrices are related in stepwise fashion from the left end to the right end to obtain the overall transfer matrix of the rotor system. The overall transfer matrix can be used to determine the steady-state responses of synchronous and superharmonic whirls of the coupling lateral and torsional vibrations. Finally, several numerical examples are presented to demonstrate the applicability of the approach.

2. Kinematics of rotating element

The orientation of the rotating element, in three-dimensional motion, can be completely described using Euler’s angles defined via three successive rotations to specify the relations between the principal axes of the rotating frame and the fixed frame. As shown in Fig. 1(a), the rotating sequence for defining Euler’s angles is explained via the following steps: (1) rotate the initial system, parallel to fixed coordinates, into a deflected mode by an angle ϕ about the Z -axis, (2) rotate the intermediate axes $(XYZ)'$ by an angle θ about the X' -axis (the so-called nodal axis) to another intermediate axes $(UVW)'$, (3) rotate intermediate axes $(UVW)'$ by an angle ψ about the W' -axis to produce the principal coordinates UVW . The Euler’s angles ϕ , θ , and ψ fully characterize the orientation of the rotating element at any given instant.

When a rotating element is deflected in position and orientation as illustrated in Fig. 1(b), the inclined angle θ of orientation is measured counterclockwise from the fixed axis Z to the spin axis W of the rotating element. In the projection description, the deflected angles (or angular displacements) are the projections of the inclined angle θ , thus $\theta_x = \theta \cos \phi$ and $\theta_y = \theta \sin \phi$. Additionally, the spin angle about the axis W is obtained as $\Phi = \phi + \psi$ from the geometric configuration of the rotating element with a very small oblique angle θ .

Through the coordinate transformation, the components of the angular velocities in the directions of principal axes can be found to be

$$\begin{bmatrix} \omega_u \\ \omega_v \\ \omega_w \end{bmatrix} = \begin{bmatrix} \cos \psi & \sin \psi & 0 \\ -\sin \psi & \cos \psi & 0 \\ 0 & 0 & 1 \end{bmatrix} \begin{bmatrix} 1 & 0 & 0 \\ 0 & \cos \theta & \sin \theta \\ 0 & -\sin \theta & \cos \theta \end{bmatrix} \begin{bmatrix} \cos \phi & \sin \phi & 0 \\ -\sin \phi & \cos \phi & 0 \\ 0 & 0 & 1 \end{bmatrix} \begin{bmatrix} 0 \\ 0 \\ \dot{\phi} \end{bmatrix} \\ + \begin{bmatrix} \cos \psi & \sin \psi & 0 \\ -\sin \psi & \cos \psi & 0 \\ 0 & 0 & 1 \end{bmatrix} \begin{bmatrix} 1 & 0 & 0 \\ 0 & \cos \theta & \sin \theta \\ 0 & -\sin \theta & \cos \theta \end{bmatrix} \begin{bmatrix} \dot{\theta} \\ 0 \\ 0 \end{bmatrix} + \begin{bmatrix} \cos \psi & \sin \psi & 0 \\ -\sin \psi & \cos \psi & 0 \\ 0 & 0 & 1 \end{bmatrix} \begin{bmatrix} 0 \\ 0 \\ \dot{\psi} \end{bmatrix},$$

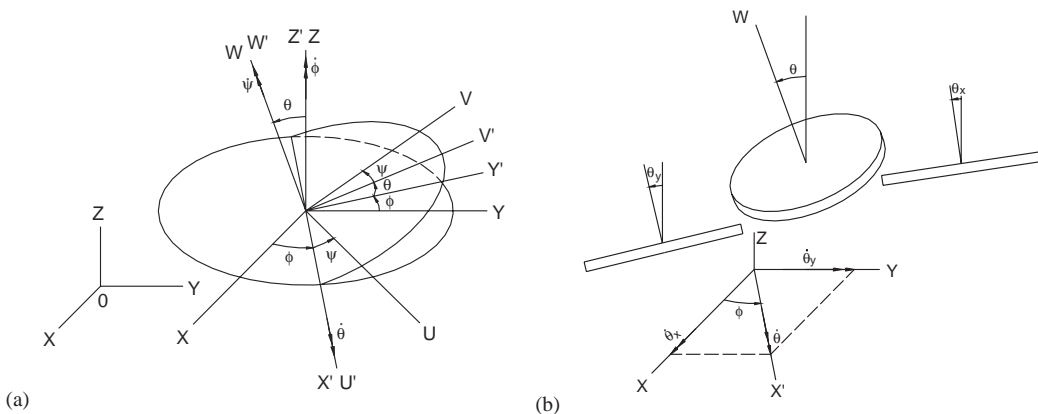


Fig. 1. Orientation of the rotating element.

that is,

$$\begin{aligned} \omega_u &= \dot{\theta} \cos \psi + \dot{\phi} \sin \theta \sin \psi, \\ \omega_v &= -\dot{\theta} \sin \psi + \dot{\phi} \sin \theta \cos \psi, \\ \omega_w &= \dot{\psi} + \dot{\phi} \cos \theta. \end{aligned} \tag{1}$$

Using principal axes, the kinetic energy E_k of a rotating element moving in three-dimensions is given by

$$E_k = \frac{1}{2}m(\dot{x}_c^2 + \dot{y}_c^2) + \frac{1}{2}(I_u\omega_u^2 + I_v\omega_v^2 + I_p\omega_w^2). \tag{2}$$

Notably the kinetic energy E_k of Eq. (2) includes two parts, one associated with the motion of the mass center, and the other associated with the angular velocities of the rotating element.

Substituting Eq. (1), $I = I_u = I_v$, $\theta_x = \theta \cos \phi$, $\theta_y = \theta \sin \phi$, $\Phi = \phi + \psi$, and $\dot{\Phi} = \dot{\phi} + \dot{\psi}$ into Eq. (2), the kinetic energy of the symmetric rotating element in the fixed frame is obtained as

$$E_k = \frac{1}{2}[m(\dot{x}_c^2 + \dot{y}_c^2) + I_p\dot{\Phi}^2 + I_p\dot{\Phi}(\dot{\theta}_x \cdot \theta_y - \dot{\theta}_y \cdot \theta_x) + I(\dot{\theta}_x^2 + \dot{\theta}_y^2)]. \tag{3}$$

The kinetic energy in the form of Eq. (3), was used by Greenhill et al. [33] to investigate rotor-bearing systems with a symmetric shaft and symmetric disks at a constant speed.

3. Transfer matrix of the rigid disk

The disk is assumed to be rigid, thin, and symmetric. Fig. 2 shows the whirling orbit of the disk with mass imbalance. The geometric relations yield

$$\begin{bmatrix} x_c \\ y_c \end{bmatrix} = \begin{bmatrix} x \\ y \end{bmatrix} + \begin{bmatrix} e_x^d \\ e_y^d \end{bmatrix} \tag{4}$$

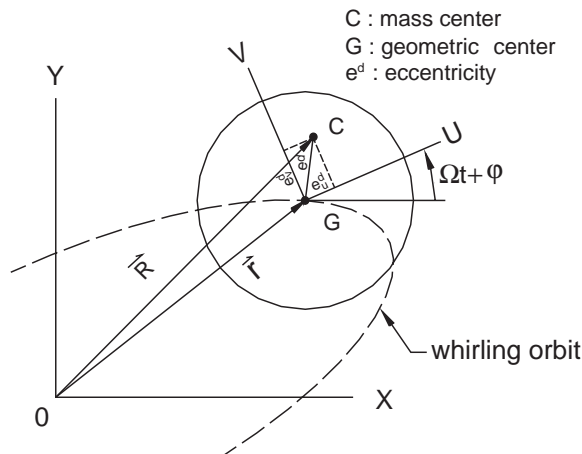


Fig. 2. Whirling orbit of the disk.

and

$$\begin{bmatrix} e_x^d \\ e_y^d \end{bmatrix} = \begin{bmatrix} \cos(\Omega t + \varphi) & -\sin(\Omega t + \varphi) \\ \sin(\Omega t + \varphi) & \cos(\Omega t + \varphi) \end{bmatrix} \begin{bmatrix} e_u^d \\ e_v^d \end{bmatrix}. \tag{5}$$

Substituting Eq. (5) into Eq. (4) and differentiating it, following relations are obtained:

$$\dot{x}_c = \dot{x} - e_v^d(\Omega + \dot{\varphi}) \cos(\Omega t + \varphi) - e_u^d(\Omega + \dot{\varphi}) \sin(\Omega t + \varphi), \tag{6}$$

$$\dot{y}_c = \dot{y} + e_u^d(\Omega + \dot{\varphi}) \cos(\Omega t + \varphi) - e_v^d(\Omega + \dot{\varphi}) \sin(\Omega t + \varphi). \tag{7}$$

Inserting Eqs. (6)–(7) and $\Phi = \Omega t + \varphi$ into Eq. (3), the kinetic energy of the symmetric disk is obtained by

$$\begin{aligned} E_k = & \frac{1}{2} m^d [\dot{x}^2 - 2\dot{x}e_v^d(\Omega + \dot{\varphi}) \cos(\Omega t + \varphi) - 2\dot{x}e_u^d(\Omega + \dot{\varphi}) \sin(\Omega t + \varphi) + \dot{y}^2 \\ & + 2\dot{y}e_u^d(\Omega + \dot{\varphi}) \cos(\Omega t + \varphi) - 2\dot{y}e_v^d(\Omega + \dot{\varphi}) \sin(\Omega t + \varphi) + (\Omega + \dot{\varphi})^2 (e^d)^2] \\ & + \frac{1}{2} I_p^d (\Omega + \dot{\varphi})^2 + \frac{1}{2} I_p^d (\Omega + \dot{\varphi}) (\dot{\theta}_x \theta_y - \dot{\theta}_y \theta_x) + \frac{1}{2} I^d (\dot{\theta}_x^2 + \dot{\theta}_y^2). \end{aligned}$$

Fig. 3 illustrates that the work done by the disk weight, bending moments, shear forces, and the torque on the left and right of the disk is

$$W = -w^d y + V_x^R x + M_y^R \theta_y + V_y^R y + M_x^R \theta_x + T^R \varphi - (V_x^L x + M_y^L \theta_y + V_y^L y + M_x^L \theta_x + T^L \varphi).$$

Using Hamilton’s principle

$$\delta \int_{t_1}^{t_2} (E_k - E_p + W) dt = 0 \tag{8}$$

and assuming small twist angle displacement, the force equilibrium equations of the disk in the fixed coordinates can be obtained as follows:

$$\begin{aligned} V_x^R - V_x^L + m^d [-\ddot{x} + \ddot{\varphi} e_v^d \cos(\Omega t + \varphi) + \ddot{\varphi} e_u^d \sin(\Omega t + \varphi) - e_v^d (\Omega + \dot{\varphi})^2 \sin(\Omega t + \varphi) \\ + e_u^d (\Omega + \dot{\varphi})^2 \cos(\Omega t + \varphi)] = 0, \end{aligned} \tag{9}$$

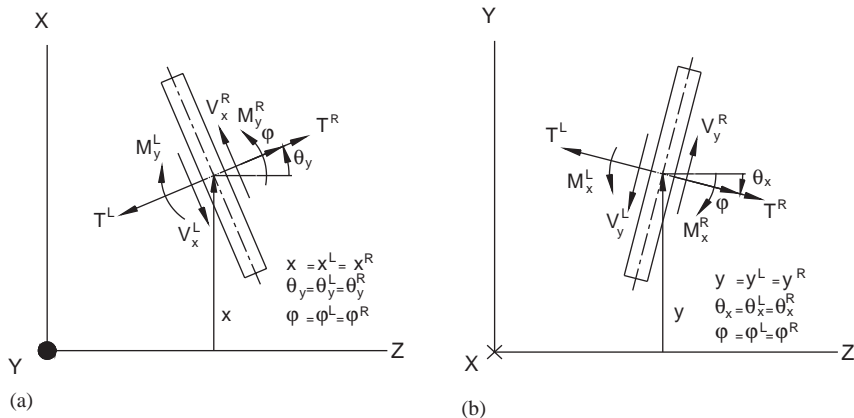


Fig. 3. Forces, moments, and torques acting on the disk.

$$V_y^R - V_y^L + m^d[-\ddot{y} - \ddot{\varphi}e_u^d \cos(\Omega t + \varphi) + \ddot{\varphi}e_v^d \sin(\Omega t + \varphi) + e_u^d(\Omega + \dot{\varphi})^2 \sin(\Omega t + \varphi) + e_v^d(\Omega + \dot{\varphi})^2 \cos(\Omega t + \varphi)] - w^d = 0, \quad (10)$$

where

$$m^d[\ddot{\varphi}e_v^d \cos(\Omega t + \varphi) + \ddot{\varphi}e_u^d \sin(\Omega t + \varphi) - e_v^d(\Omega + \dot{\varphi})^2 \sin(\Omega t + \varphi) + e_u^d(\Omega + \dot{\varphi})^2 \cos(\Omega t + \varphi)]$$

and

$$m^d[-\ddot{\varphi}e_u^d \cos(\Omega t + \varphi) + \ddot{\varphi}e_v^d \sin(\Omega t + \varphi) + e_u^d(\Omega + \dot{\varphi})^2 \sin(\Omega t + \varphi) + e_v^d(\Omega + \dot{\varphi})^2 \cos(\Omega t + \varphi)]$$

are the unbalance forces of the disk in the x and y directions, respectively. The twist angle (φ) and its derivatives affect the level of the unbalance force of the disk.

The bending moment equilibrium equations in the fixed coordinates are

$$M_x^R - M_x^L - I^d \ddot{\theta}_x - \frac{1}{2} I_p^d \ddot{\varphi} \theta_y - I_p^d (\Omega + \dot{\varphi}) \dot{\theta}_y = 0, \quad (11)$$

$$M_y^R - M_y^L - I^d \ddot{\theta}_y + \frac{1}{2} I_p^d \ddot{\varphi} \theta_x + I_p^d (\Omega + \dot{\varphi}) \dot{\theta}_x = 0, \quad (12)$$

where $\frac{1}{2} I_p^d \ddot{\varphi} \theta_y$ and $\frac{1}{2} I_p^d \ddot{\varphi} \theta_x$ are the moments coupled with the twist acceleration ($\ddot{\varphi}$), $I_p^d (\Omega + \dot{\varphi}) \dot{\theta}_y$ and $I_p^d (\Omega + \dot{\varphi}) \dot{\theta}_x$ the gyroscopic moments coupled with the twist velocity ($\dot{\varphi}$).

The torque equilibrium equations in the fixed coordinates is

$$T^R - T^L - I_p^d \ddot{\varphi} - \frac{1}{2} I_p^d \ddot{\theta}_x \theta_y + \frac{1}{2} I_p^d \ddot{\theta}_y \theta_x + m^d[\ddot{x}e_v^d \cos(\Omega t + \varphi) + \ddot{x}e_u^d \sin(\Omega t + \varphi) - \ddot{y}e_u^d \cos(\Omega t + \varphi) + \ddot{y}e_v^d \sin(\Omega t + \varphi) - (e^d)^2 \ddot{\varphi}] = 0, \quad (13)$$

where $\frac{1}{2} I_p^d \ddot{\theta}_x \theta_y$ and $\frac{1}{2} I_p^d \ddot{\theta}_y \theta_x$ are the torques coupled with bending angle and angular acceleration, and

$$m^d[\ddot{x}e_v^d \cos(\Omega t + \varphi) + \ddot{x}e_u^d \sin(\Omega t + \varphi) - \ddot{y}e_u^d \cos(\Omega t + \varphi) + \ddot{y}e_v^d \sin(\Omega t + \varphi) - (e^d)^2 \ddot{\varphi}]$$

is the torque induced by the unbalance force.

Eqs. (9)–(13) can be simplified into motion equations of the simple Jeffcott rotor [31,32]. In the simple Jeffcott rotor, the unbalanced disk is located at the middle of the shaft, and only its lateral and torsional motion is allowed. Gyroscopic and rotary inertia effects are neglected, i.e., Eqs. (11) and (12) vanish. The coupling terms $\frac{1}{2} I_p^d \ddot{\theta}_x \theta_y$ and $\frac{1}{2} I_p^d \ddot{\theta}_y \theta_x$ in Eq. (13) also disappear. If the shear forces and torques are replaced by the lateral stiffness forces and torsional stiffness torques of the shaft, respectively, Eqs. (9)–(10) and (13) become

$$k^s x + m^d[-\ddot{x} + \ddot{\varphi}e_v^d \cos(\Omega t + \varphi) + \ddot{\varphi}e_u^d \sin(\Omega t + \varphi) - e_v^d(\Omega + \dot{\varphi})^2 \sin(\Omega t + \varphi) + e_u^d(\Omega + \dot{\varphi})^2 \cos(\Omega t + \varphi)] = 0,$$

$$k^s y + m^d[-\ddot{y} - \ddot{\varphi}e_u^d \cos(\Omega t + \varphi) + \ddot{\varphi}e_v^d \sin(\Omega t + \varphi) + e_u^d(\Omega + \dot{\varphi})^2 \sin(\Omega t + \varphi) + e_v^d(\Omega + \dot{\varphi})^2 \cos(\Omega t + \varphi)] - w^d = 0,$$

$$k_{\varphi}^s \varphi - I_p^d \ddot{\varphi} + m^d [\ddot{x} e_v^d \cos(\Omega t + \varphi) + \ddot{x} e_u^d \sin(\Omega t + \varphi) - \ddot{y} e_u^d \cos(\Omega t + \varphi) + \ddot{y} e_v^d \sin(\Omega t + \varphi) - (e^d)^2 \ddot{\varphi}] = 0,$$

where k^s denotes the shaft lateral stiffness and k_{φ}^s represents the shaft torsional stiffness. The above motion equations are the same as those in Refs. [31,32].

The compatible relations between the two sides of the disk are given by

$$x^R = x^L, \quad y^R = y^L, \quad \theta_x^R = \theta_x^L, \quad \theta_y^R = \theta_y^L, \quad \varphi^R = \varphi^L. \quad (14)$$

For a nonlinear differential equation, Hayashi [34] introduced the harmonic balance method for obtaining the solution of a higher approximation as follows. The solution was first expanded into Fourier series with unknown coefficients. The assumed solution was then inserted into the original equation, and the sine and cosine terms of the respective frequencies were set to zero. Solving the simultaneous equations thus obtained can identify the unknown coefficients of the assumed solution. The harmonic balance method has been utilized by Kang et al. [7,21].

Using the harmonic balance method, the steady-state responses of Eqs. (9)–(14) can each be expressed in Fourier series form as

$$x(t) = x_0 + \sum_{i=1}^n x_{ic} \cos i\Omega t + x_{is} \sin i\Omega t,$$

$$y(t) = y_0 + \sum_{i=1}^n y_{ic} \cos i\Omega t + y_{is} \sin i\Omega t,$$

$$\theta_x(t) = \theta_{x,0} + \sum_{i=1}^n \theta_{x,ic} \cos i\Omega t + \theta_{x,is} \sin i\Omega t,$$

$$\theta_y(t) = \theta_{y,0} + \sum_{i=1}^n \theta_{y,ic} \cos i\Omega t + \theta_{y,is} \sin i\Omega t,$$

$$\varphi(t) = \varphi_0 + \sum_{i=1}^n \varphi_{ic} \cos i\Omega t + \varphi_{is} \sin i\Omega t. \quad (15)$$

Other variables can be similarly expressed as

$$V_x(t) = V_{x,0} + \sum_{i=1}^n V_{x,ic} \cos i\Omega t + V_{x,is} \sin i\Omega t,$$

$$V_y(t) = V_{y,0} + \sum_{i=1}^n V_{y,ic} \cos i\Omega t + V_{y,is} \sin i\Omega t,$$

$$M_x(t) = M_{x,0} + \sum_{i=1}^n M_{x,ic} \cos i\Omega t + M_{x,is} \sin i\Omega t,$$

$$M_y(t) = M_{y,0} + \sum_{i=1}^n M_{y,ic} \cos i\Omega t + M_{y,is} \sin i\Omega t,$$

$$T(t) = T_0 + \sum_{i=1}^n T_{ic} \cos i\Omega t + T_{is} \sin i\Omega t. \tag{16}$$

Using the relations

$$\cos(\Omega t + \varphi) = \cos \Omega t \cos \varphi - \sin \Omega t \sin \varphi \approx \cos \Omega t - \varphi \sin \Omega t,$$

$$\sin(\Omega t + \varphi) = \sin \Omega t \cos \varphi + \cos \Omega t \sin \varphi \approx \sin \Omega t + \varphi \cos \Omega t$$

substituting Eqs. (15) and (16) into Eqs. (9)–(14), ignoring the nonlinear terms, and equating the coefficients of the same harmonic term provides the transfer matrix equation of the disk for static, synchronous whirl and nonsynchronous whirls in the static frame:

$$\begin{bmatrix} \mathbf{S}^R \\ 1 \end{bmatrix} = [T^d]_{k \times k} \begin{bmatrix} \mathbf{S}^L \\ 1 \end{bmatrix}, \tag{17}$$

where $k = 20n + 11$ and the state variable vector \mathbf{S} is denoted as

$$\mathbf{S} = \begin{bmatrix} \mathbf{X} \\ \mathbf{F} \end{bmatrix}, \tag{18}$$

where

$$\mathbf{X} = [x_0 \ x_{1c} \ \dots \ x_{nc} \ x_{1s} \ \dots \ x_{ns} \ y_0 \ y_{1c} \ \dots \ y_{nc} \ y_{1s} \ \dots \ y_{ns} \ \theta_{x,0} \ \theta_{x,1c} \ \dots \ \theta_{x,nc} \ \theta_{x,1s} \ \dots \ \theta_{x,ns} \ \theta_{y,0} \ \theta_{y,1c} \ \dots \ \theta_{y,nc} \ \theta_{y,1s} \ \dots \ \theta_{y,ns} \ \varphi_0 \ \varphi_{1c} \ \dots \ \varphi_{nc} \ \varphi_{1s} \ \dots \ \varphi_{ns}]^T$$

and

$$\mathbf{F} = [V_{x,0} \ V_{x,1c} \ \dots \ V_{x,nc} \ V_{x,1s} \ \dots \ V_{x,ns} \ V_{y,0} \ V_{y,1c} \ \dots \ V_{y,nc} \ V_{y,1s} \ \dots \ V_{y,ns} \ M_{x,0} \ M_{x,1c} \ \dots \ M_{x,nc} \ M_{x,1s} \ \dots \ M_{x,ns} \ M_{y,0} \ M_{y,1c} \ \dots \ M_{y,nc} \ M_{y,1s} \ \dots \ M_{y,ns} \ T_0 \ T_{1c} \ \dots \ T_{nc} \ T_{1s} \ \dots \ T_{ns}]^T.$$

4. Transfer matrix of Timoshenko shaft

As shown in Fig. 4, the finite shaft element can be considered to comprise numerous small rotating elements. Thus the total kinetic energy of the shaft element is the sum of these kinetic energies of the rotating elements. Using a similar procedure to that illustrated in Section 3, the kinetic energy of the symmetric shaft element expressed in fixed coordinates is

$$E_k = \frac{1}{2} \rho \int_0^L \{A[\dot{x}^2 - 2\dot{x}e_v^s(\Omega + \dot{\varphi}) \cos(\Omega t + \varphi) - 2\dot{x}e_u^s(\Omega + \dot{\varphi}) \sin(\Omega t + \varphi) + \dot{y}^2 + 2\dot{y}e_u^s(\Omega + \dot{\varphi}) \cos(\Omega t + \varphi) - 2\dot{y}e_v^s(\Omega + \dot{\varphi}) \sin(\Omega t + \varphi) + (\Omega + \dot{\varphi})^2(e^s)^2] + I_p^s(\Omega + \dot{\varphi})^2 + I_p^s(\Omega + \dot{\varphi})(\dot{\theta}_x\theta_y - \dot{\theta}_y\theta_x) + I^s(\dot{\theta}_x^2 + \dot{\theta}_y^2)\} dZ. \tag{19}$$

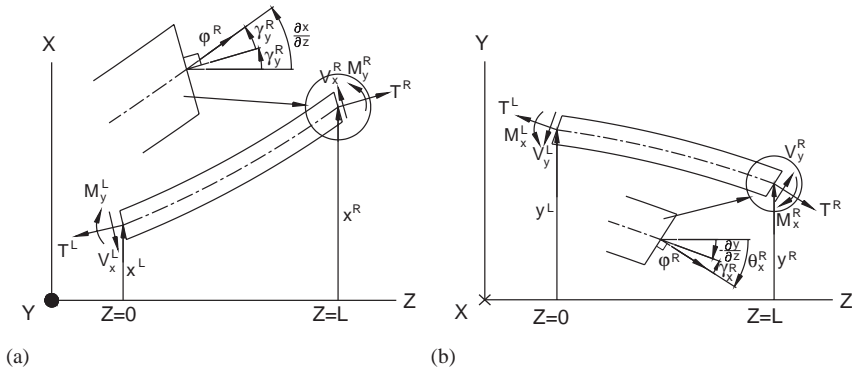


Fig. 4. Forces, moments, and torques acting on the finite shaft element.

The total potential energy according to the bending and shear deformations can be expressed in fixed coordinates as in Kang et al. [6]

$$E_p = \frac{1}{2} \int_0^L [EI^s(\theta'_x)^2 + EI^s(\theta'_y)^2 + k_s GA(\gamma_x^2 + \gamma_y^2) + GI_p^s(\phi')^2] dZ. \tag{20}$$

The work done by the external force (see Fig. 4) is

$$W = \int_0^L -\rho A g y dZ + V_x^R x + M_y^R \theta_y + V_y^R y + M_x^R \theta_x + T^R \phi - (V_x^L x + M_y^L \theta_y + V_y^L y + M_x^L \theta_x + T^L \phi). \tag{21}$$

Using Hamilton’s principle and assuming small twist angle displacement, this study obtains the force equilibrium equations of the shaft in the fixed coordinates:

$$-\rho A \ddot{x} + \rho A [\ddot{\phi} e_v^s \cos(\Omega t + \phi) + \ddot{\phi} e_u^s \sin(\Omega t + \phi) - (\Omega + \dot{\phi})^2 e_v^s \sin(\Omega t + \phi) + (\Omega + \dot{\phi})^2 e_u^s \cos(\Omega t + \phi)] + k_s GA(x'' - \theta'_y) = 0, \tag{22}$$

$$-\rho A \ddot{y} + \rho A [-\ddot{\phi} e_u^s \cos(\Omega t + \phi) + \ddot{\phi} e_v^s \sin(\Omega t + \phi) + (\Omega + \dot{\phi})^2 e_u^s \sin(\Omega t + \phi) + (\Omega + \dot{\phi})^2 e_v^s \cos(\Omega t + \phi)] + k_s GA(\theta'_x + y'') - \rho A g = 0. \tag{23}$$

From above equations, the twist angle (ϕ) and its derivatives can be found to emerge from the unbalance forces:

$$\rho A [\ddot{\phi} e_v^s \cos(\Omega t + \phi) + \ddot{\phi} e_u^s \sin(\Omega t + \phi) - (\Omega + \dot{\phi})^2 e_v^s \sin(\Omega t + \phi) + (\Omega + \dot{\phi})^2 e_u^s \cos(\Omega t + \phi)]$$

and

$$\rho A [-\ddot{\phi} e_u^s \cos(\Omega t + \phi) + \ddot{\phi} e_v^s \sin(\Omega t + \phi) + (\Omega + \dot{\phi})^2 e_u^s \sin(\Omega t + \phi) + (\Omega + \dot{\phi})^2 e_v^s \cos(\Omega t + \phi)]$$

and influence the level of the unbalance forces.

The bending moment equilibrium equations in the fixed coordinates are

$$\rho I^s \ddot{\theta}_x + \frac{1}{2} \rho I_p^s \ddot{\phi} \theta_y + \rho I_p^s (\Omega + \dot{\phi}) \dot{\theta}_y - EI^s \theta_x'' + k_s GA(\theta_x + y') = 0, \tag{24}$$

$$\rho I^s \ddot{\theta}_y - \frac{1}{2} \rho I_p^s \ddot{\phi} \theta_x - \rho I_p^s (\Omega + \dot{\phi}) \dot{\theta}_x - EI^s \theta_y'' + k_s GA(\theta_y - x') = 0, \tag{25}$$

where $\frac{1}{2} \rho I_p^s \ddot{\phi} \theta_y$ and $\frac{1}{2} \rho I_p^s \ddot{\phi} \theta_x$ denote the moments coupled with the twist acceleration ($\ddot{\phi}$), $\rho I_p^s (\Omega + \dot{\phi}) \dot{\theta}_y$ and $\rho I_p^s (\Omega + \dot{\phi}) \dot{\theta}_x$ represent the gyroscopic moments coupled with the twist velocity ($\dot{\phi}$).

The torque equilibrium equation in the fixed coordinates is

$$\begin{aligned} &\rho I_p^s \ddot{\phi} + \frac{1}{2} \rho I_p^s \ddot{\theta}_x \theta_y - \frac{1}{2} \rho I_p^s \ddot{\theta}_y \theta_x + \rho A [-\ddot{x}e_v^s \cos(\Omega t + \phi) - \ddot{x}e_u^s \sin(\Omega t + \phi) \\ &+ \ddot{y}e_u^s \cos(\Omega t + \phi) - \ddot{y}e_v^s \sin(\Omega t + \phi) + (e^s)^2 \ddot{\phi}] - GI_p^s \phi'' = 0, \end{aligned} \tag{26}$$

where $\frac{1}{2} \rho I_p^s \ddot{\theta}_x \theta_y$ and $\frac{1}{2} \rho I_p^s \ddot{\theta}_y \theta_x$ are the torques coupled by bending angle and angular acceleration, and

$$\rho A [-\ddot{x}e_v^s \cos(\Omega t + \phi) - \ddot{x}e_u^s \sin(\Omega t + \phi) + \ddot{y}e_u^s \cos(\Omega t + \phi) - \ddot{y}e_v^s \sin(\Omega t + \phi) + (e^s)^2 \ddot{\phi}]$$

is the torque induced by unbalance force.

The natural boundary conditions are

$$\begin{aligned} &V_x^R + [k_s GA(\theta_y - x')]_{Z=L} = 0, \quad V_x^L + [k_s GA(\theta_y - x')]_{Z=0} = 0, \\ &V_y^R + [-k_s GA(\theta_x + y')]_{Z=L} = 0, \quad V_y^L + [-k_s GA(\theta_x + y')]_{Z=0} = 0, \\ &M_x^R + [-EI^s \theta_x']_{Z=L} = 0, \quad M_x^L + [-EI^s \theta_x']_{Z=0} = 0, \\ &M_y^R + [-EI^s \theta_y']_{Z=L} = 0, \quad M_y^L + [-EI^s \theta_y']_{Z=0} = 0, \\ &T^R + [-GI_p^s \phi']_{Z=L} = 0, \quad T^L + [-GI_p^s \phi']_{Z=0} = 0. \end{aligned} \tag{27}$$

The steady-state solution of Eqs. (22)–(26) can be expressed in Fourier series form as

$$\begin{aligned} x(Z, t) &= x_0(Z) + \sum_{i=1}^n x_{ic}(Z) \cos i\Omega t + x_{is}(Z) \sin i\Omega t, \\ y(Z, t) &= y_0(Z) + \sum_{i=1}^n y_{ic}(Z) \cos i\Omega t + y_{is}(Z) \sin i\Omega t, \\ \theta_x(Z, t) &= \theta_{x,0}(Z) + \sum_{i=1}^n \theta_{x,ic}(Z) \cos i\Omega t + \theta_{x,is}(Z) \sin i\Omega t, \\ \theta_y(Z, t) &= \theta_{y,0}(Z) + \sum_{i=1}^n \theta_{y,ic}(Z) \cos i\Omega t + \theta_{y,is}(Z) \sin i\Omega t, \\ \phi(Z, t) &= \phi_0(Z) + \sum_{i=1}^n \phi_{ic}(Z) \cos i\Omega t + \phi_{is}(Z) \sin i\Omega t, \end{aligned} \tag{28}$$

where $x_0(Z)$, $y_0(Z)$, $\theta_{x,0}(Z)$, $\theta_{y,0}(Z)$, $\varphi_0(z)$, $x_{ic}(Z)$, $x_{is}(Z)$, $y_{ic}(Z)$, $y_{is}(Z)$, $\theta_{x,ic}(Z)$, $\theta_{x,is}(Z)$, $\theta_{y,ic}(Z)$, $\theta_{y,is}(Z)$, $\varphi_{ic}(z)$ and $\varphi_{is}(z)$ are the mode functions of the relative 0th order and $n \times$ harmonic whirl with respect to the static frame of the shaft. For convenience, the mode function vector of general displacement are denoted as $\mathbf{X}(Z)$, namely

$$\mathbf{X}(Z) = [x_0(Z)x_{1c}(Z) \cdots x_{nc}(Z)x_{1s}(Z) \cdots x_{ns}(Z)y_0(Z)y_{1c}(Z) \cdots y_{nc}(Z)y_{1s}(Z) \cdots y_{ns}(Z) \theta_{x,0}(Z)\theta_{x,1c}(Z) \cdots \theta_{x,nc}(Z)\theta_{x,1s}(Z) \cdots \theta_{x,ns}(Z)\theta_{y,0}(Z)\theta_{y,1c}(Z) \cdots \theta_{y,nc}(Z)\theta_{y,1s}(Z) \cdots \theta_{y,ns}(Z) \varphi_0(Z)\varphi_{1c}(Z) \cdots \varphi_{nc}(Z)\varphi_{1s}(Z) \cdots \varphi_{ns}(Z)]^T \tag{29}$$

Substituting Eq. (28) into Eqs. (22)–(26), ignoring the nonlinear terms, and equating the coefficients of the same harmonic term produces 33 nonhomogeneous differential equations as listed in Appendix A. The general solutions of the nonhomogeneous system, Eqs. (A.1)–(A.33), can be represented by the sum of the homogeneous and the particular solutions, namely

$$\mathbf{X}(Z) = \mathbf{X}(Z)^h + \mathbf{X}(Z)^p \tag{30}$$

Assume the homogeneous solution $\mathbf{X}(Z)^h$ in the forms

$$\mathbf{X}(Z)^h = \mathbf{X}^h e^{\lambda Z}, \tag{31}$$

where the arbitrary constant vector $\mathbf{X}^h = [x_0^h \ x_{1c}^h \cdots x_{nc}^h \ x_{1s}^h \cdots x_{ns}^h \ y_0^h \ y_{1c}^h \cdots y_{nc}^h \ y_{1s}^h \cdots y_{ns}^h \ \theta_{x,0}^h \ \theta_{x,1c}^h \cdots \theta_{x,nc}^h \ \theta_{x,1s}^h \cdots \theta_{x,ns}^h \ \theta_{y,0}^h \ \theta_{y,1c}^h \cdots \theta_{y,nc}^h \ \theta_{y,1s}^h \cdots \theta_{y,ns}^h \ \varphi_0^h \ \varphi_{1c}^h \cdots \varphi_{nc}^h \ \varphi_{1s}^h \cdots \varphi_{ns}^h]^T$ and λ is the characteristic value, with respect to a nature mode.

Substituting Eq. (31) into Eqs. (A.1)–(A.33) yields the following characteristic equation:

$$(\lambda^2 \mathbf{E}_2 + \lambda \mathbf{E}_1 + \mathbf{E}_0) \mathbf{X}^h, \tag{32}$$

where \mathbf{E}_2 , \mathbf{E}_1 and \mathbf{E}_0 are matrices with size $(10n + 5) \times (10n + 5)$ and are listed in Appendix B. Eq. (32) can be rewritten as the generalized eigen-problem form

$$\left\{ \lambda \begin{bmatrix} \mathbf{0} & \mathbf{E}_2 \\ \mathbf{E}_2 & \mathbf{E}_1 \end{bmatrix}_{k \times k} - \begin{bmatrix} \mathbf{E}_2 & \mathbf{0} \\ \mathbf{0} & -\mathbf{E}_0 \end{bmatrix}_{k \times k} \right\} \begin{bmatrix} \lambda \mathbf{X}^h \\ \mathbf{X}^h \end{bmatrix}_{k \times 1} = \begin{bmatrix} \mathbf{0} \\ \mathbf{0} \end{bmatrix}_{k \times 1}, \tag{33}$$

where $k = 20n + 10$.

By solving Eq. (33), the eigen-value λ and corresponding eigenvector \mathbf{X}^h are obtained. Hence the homogeneous solution is

$$\mathbf{X}(Z)^h = \sum_{i=1}^{20n+10} C_i \mathbf{X}_i^h e^{\lambda_i Z}, \tag{34}$$

where C_i is an undetermined constant, and \mathbf{X}_i^h is the eigenvector corresponding to λ_i .

From Eqs. (A.3), (A.2), (A.10)–(A.12) and (A.19), the following particular solutions are obtained

$$\begin{aligned} x_{1s}^p &= e_v^s, & x_{1c}^p &= -e_u^s, & y_{1s}^p &= -e_u^s, & y_{1c}^p &= -e_v^s, \\ y_0^p &= \frac{\rho Ag}{2k_s G} Z^2 - \frac{\rho Ag}{24EI^s} Z^4, & \theta_{x0}^p &= \frac{\rho Ag}{6EI^s} Z^3. \end{aligned} \tag{35}$$

Substituting Eqs. (34) and (35) into Eq. (30) yields

$$\mathbf{X}(Z) = [G(Z)] \begin{bmatrix} \mathbf{C} \\ 1 \end{bmatrix}, \quad (36)$$

where $[G(Z)]$ is the matrix of the function of Z with size $(10n + 5) \times (20n + 11)$ and undetermined constant vector $\mathbf{C} = [C_1 C_2 \cdots C_{20n+10}]^T$. Thus the general displacement state variable vectors can be expressed as

$$\mathbf{X}^R = \mathbf{X}(Z = L) = [G_L] \begin{bmatrix} \mathbf{C} \\ 1 \end{bmatrix}, \quad (37)$$

where $[G_L] = [G(Z = L)]$ and

$$\mathbf{X}^L = \mathbf{X}(Z = 0) = [G_0] \begin{bmatrix} \mathbf{C} \\ 1 \end{bmatrix}, \quad (38)$$

where $[G_0] = [G(Z = 0)]$.

The solutions of Eq. (27) can be expressed in Fourier series form as

$$\begin{aligned} V_x(Z, t) &= V_{x,0}(Z) + \sum_{i=1}^n V_{x,ic}(Z) \cos i\Omega t + V_{x,is}(Z) \sin i\Omega t, \\ V_y(Z, t) &= V_{y,0}(Z) + \sum_{i=1}^n V_{y,ic}(Z) \cos i\Omega t + V_{y,is}(Z) \sin i\Omega t, \\ M_x(Z, t) &= M_{x,0}(Z) + \sum_{i=1}^n M_{x,ic}(Z) \cos i\Omega t + M_{x,is}(Z) \sin i\Omega t, \\ M_y(Z, t) &= M_{y,0}(Z) + \sum_{i=1}^n M_{y,ic}(Z) \cos i\Omega t + M_{y,is}(Z) \sin i\Omega t, \\ T(Z, t) &= T_0(Z) + \sum_{i=1}^n T_{ic}(Z) \cos i\Omega t + T_{is}(Z) \sin i\Omega t. \end{aligned} \quad (39)$$

The mode function vector of the general force $\mathbf{F}(Z)$ is defined as

$$\begin{aligned} \mathbf{F}(Z) &= [V_{x,0}(Z) V_{x,1c}(Z) \cdots V_{x,nc}(Z) V_{x,1s}(Z) \cdots V_{x,ns}(Z) \\ &\quad V_{y,0}(Z) V_{y,1c}(Z) \cdots V_{y,nc}(Z) V_{y,1s}(Z) \cdots V_{y,ns}(Z) \\ &\quad M_{x,0}(Z) M_{x,1c}(Z) \cdots M_{x,nc}(Z) M_{x,1s}(Z) \cdots M_{x,ns}(Z) \\ &\quad M_{y,0}(Z) M_{y,1c}(Z) \cdots M_{y,nc}(Z) M_{y,1s}(Z) \cdots M_{y,ns}(Z) \\ &\quad T_0(Z) T_{1c}(Z) \cdots T_{nc}(Z) T_{1s}(Z) \cdots T_{ns}(Z)]^T. \end{aligned} \quad (40)$$

By inserting Eq. (39) into (27) and using Eq. (36), the mode function vector of the general force at right \mathbf{F}^R is given by

$$\mathbf{F}^R = [H_L] \begin{bmatrix} \mathbf{C} \\ 1 \end{bmatrix}, \tag{41}$$

where $[H_L]$ denotes a matrix with size $(10n + 5) \times (20n + 11)$, and the mode function vector of the general force at left \mathbf{F}^L is given by

$$\mathbf{F}^L = [H_0] \begin{bmatrix} \mathbf{C} \\ 1 \end{bmatrix}, \tag{42}$$

where $[H_0]$ is a matrix with size $(10n + 5) \times (20n + 11)$

Combining Eqs. (37), (38), (41) and (42) yields

$$\begin{bmatrix} \mathbf{S}^R \\ 1 \end{bmatrix} = [M_L] \begin{bmatrix} \mathbf{C} \\ 1 \end{bmatrix}, \tag{43}$$

where $[M_L]$ is a matrix with size $(20n + 11) \times (20n + 11)$ and

$$\begin{bmatrix} \mathbf{S}^L \\ 1 \end{bmatrix} = [M_0] \begin{bmatrix} \mathbf{C} \\ 1 \end{bmatrix}, \tag{44}$$

where $[M_0]$ is a matrix with size $(20n + 11) \times (20n + 11)$.

Using Eqs. (43) and (44), the transfer matrix $[T^s]$ of the shaft can be obtained

$$\begin{bmatrix} \mathbf{S}^R \\ 1 \end{bmatrix} = [M_L] \begin{bmatrix} \mathbf{C} \\ 1 \end{bmatrix} = [M_L][M_0]^{-1} \begin{bmatrix} \mathbf{S}^L \\ 1 \end{bmatrix} = [T^s] \begin{bmatrix} \mathbf{S}^L \\ 1 \end{bmatrix}. \tag{45}$$

The transfer matrix $[T^s]$, with size $(20n + 11) \times (20n + 11)$ is constructed to relate two sides of a uniform and symmetric Timoshenko shaft with eccentricity for the relative 0th-order static deflection, synchronous whirl, and $n \times$ whirl (n th order) in the static frame.

5. Transfer matrix of the linear bearing

In the rotor system, the bearing can be simplified into a linear element. Fig. 5 illustrates the force F_x^b, F_y^b , bending moment M_x^b, M_y^b , and torque T^b acting on the shaft due to the bearing are given by

$$\begin{bmatrix} F_x^b \\ F_y^b \end{bmatrix} = - \begin{bmatrix} K_{xx} & K_{xy} \\ K_{yx} & K_{yy} \end{bmatrix} \begin{bmatrix} x \\ y \end{bmatrix} - \begin{bmatrix} C_{xx} & C_{xy} \\ C_{yx} & C_{yy} \end{bmatrix} \begin{bmatrix} \dot{x} \\ \dot{y} \end{bmatrix},$$

$$\begin{bmatrix} M_x^b \\ M_y^b \end{bmatrix} = - \begin{bmatrix} K_{\theta xx} & K_{\theta xy} \\ K_{\theta yx} & K_{\theta yy} \end{bmatrix} \begin{bmatrix} \theta_x \\ \theta_y \end{bmatrix} - \begin{bmatrix} C_{\theta xx} & C_{\theta xy} \\ C_{\theta yx} & C_{\theta yy} \end{bmatrix} \begin{bmatrix} \dot{\theta}_x \\ \dot{\theta}_y \end{bmatrix},$$

$$T^b = -K_\varphi \varphi - C_\varphi \dot{\varphi}. \tag{46}$$

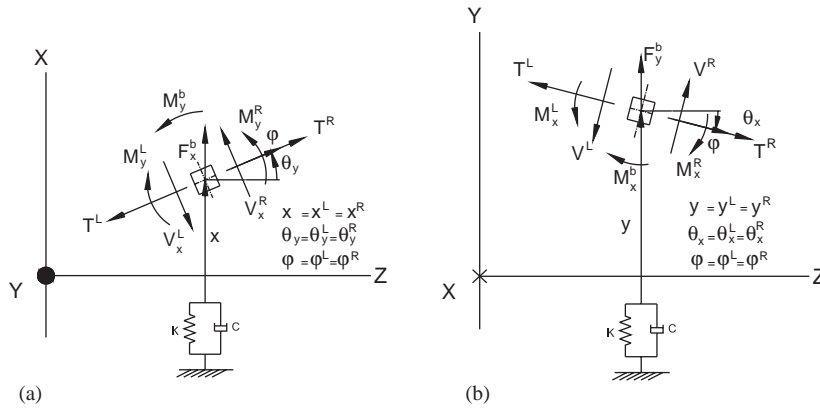


Fig. 5. Forces, moments, and torques acting on the node of the bearing.

Hence the equilibrium relations of the force, bending moment and torque acting on the shaft can be expressed as

$$\begin{bmatrix} V_x^R \\ V_y^R \end{bmatrix} = \begin{bmatrix} V_x^L \\ V_y^L \end{bmatrix} - \begin{bmatrix} F_x^b \\ F_y^b \end{bmatrix} = \begin{bmatrix} V_x^L \\ V_y^L \end{bmatrix} + \begin{bmatrix} K_{xx} & K_{xy} \\ K_{yx} & K_{yy} \end{bmatrix} \begin{bmatrix} x \\ y \end{bmatrix} + \begin{bmatrix} C_{xx} & C_{xy} \\ C_{yx} & C_{yy} \end{bmatrix} \begin{bmatrix} \dot{x} \\ \dot{y} \end{bmatrix},$$

$$\begin{bmatrix} M_x^R \\ M_y^R \end{bmatrix} = \begin{bmatrix} M_x^L \\ M_y^L \end{bmatrix} - \begin{bmatrix} M_x^b \\ M_y^b \end{bmatrix} = \begin{bmatrix} M_x^L \\ M_y^L \end{bmatrix} + \begin{bmatrix} K_{\theta xx} & K_{\theta xy} \\ K_{\theta yx} & K_{\theta yy} \end{bmatrix} \begin{bmatrix} \theta_x \\ \theta_y \end{bmatrix} + \begin{bmatrix} C_{\theta xx} & C_{\theta xy} \\ C_{\theta yx} & C_{\theta yy} \end{bmatrix} \begin{bmatrix} \dot{\theta}_x \\ \dot{\theta}_y \end{bmatrix},$$

$$T^R = T^L + K_\phi \phi + C_\phi \dot{\phi}. \tag{47}$$

Substituting the Fourier series representation of x , y , θ_x , θ_y , V_x , V_y , M_y , M_x and T into Eq. (47) and equating the coefficients of the same harmonic term, the transfer matrix of the linear bearing can be obtained as $[T^b]$

$$\begin{bmatrix} \mathbf{S}^R \\ 1 \end{bmatrix} = [T^b]_{k \times k} \begin{bmatrix} \mathbf{S}^L \\ 1 \end{bmatrix}, \tag{48}$$

where $k = 20n + 11$. The state variable vector \mathbf{S} contains the total coefficient of the Fourier series from static variables to the n th-order harmonic term.

6. Overall transfer matrix of the whole system

Fig. 6 shows that the typical system has multi-disks, bearings and a flexible shaft with a torque at the right end. The overall transfer matrix of the rotor system is the relation between the two ends of the shaft, and can be derived by stepwise relationship of the state vectors from the left end to the right end. The multiplication of the matrices of all elements from the left to the right end

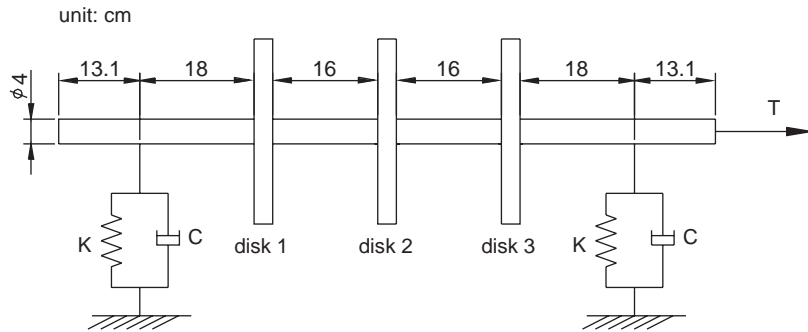


Fig. 7. System for the numerical examples.

7. Numerical examples

To demonstrate the applicability of this approach and show the effects of mass unbalance and external torque on the steady-state vibration, a rotor-bearing system with the symmetric shaft is used, as illustrated in Fig. 7. The response amplitude is defined as the maximum flexural displacement, i.e.,

$$\text{Amplitude} = \text{maximum value of } \sqrt{x(t)^2 + y(t)^2}.$$

The systems supported by the isotropic and anisotropic bearings are analyzed individually. Table 1 lists the details of the rotor-bearing systems.

Case 1: Isotropic rotor-bearing system: If no external torque but only the unbalance force is acting on the system, the whirling orbit is forward, synchronous, and right circular (Fig. 8). A synchronous lateral mode occurs at 3024 rev/min and the amplitude becomes increases at this rotating speed. Fig. 9 illustrates the response amplitudes excited by the different $1\times$ torques along with the unbalance force, and the orbits of disk 1 when torque = $5000 \cos \Omega t$ Nm. Two peaks other than synchronous resonance clearly appear. With increasing the amount of external torque, the amplitudes of the added resonant peaks increase, and the positions of the resonant peaks become irrelevant to the amount of the external torque. This behavior implies that the amount of external torque cannot alter the rotor nature frequency. The whirling orbits excited by both the unbalance force and external torque are forward but not necessarily synchronous and right circular. The whirling orbit is double-looped at 1490 and 2530 rev/min, and is roughly circular at 3050 rev/min (near the lateral resonant frequency 3024 rev/min).

Fig. 10 shows the response amplitudes of the components for torque = $5000 \cos \Omega t$ Nm. The response is composed of synchronous (i.e., $1\times$) and $2\times$ whirls. Notably, the synchronous component is the same as in Fig. 9 for $T = 0$. Accordingly, the unbalance force, with $1\times$ exciting frequency, is known to excite the synchronous component. The torque excites the torsional vibration with torsional exciting frequency and, under the system coupling effect, also stimulates the lateral vibration whose whirly frequency is that of the torque plus or minus the rotating speed. Thus, owing to the coupling effect of the rotor system, the $1\times$ torque excites a $2\times$ lateral mode at 1497.3 rev/min, which is a half of the lateral resonant frequency (3024 rev/min), and

Table 1
Details of the three-disk rotor system

The coefficients of the shaft	
E	$207 \times 10^9 \text{ N/m}^2$
G	$81 \times 10^9 \text{ N/m}^2$
k_s	0.68
ρ	7750 kg/m^3
e_u^s	$2 \times 10^{-5} \text{ m}$
e_v^s	0
The coefficients of the disks	
m^d	13.47 kg
I_p^d	$1020 \times 10^{-4} \text{ kg m}^2$
I^d	$512 \times 10^{-4} \text{ kg m}^2$
e_u^d of the disk 1	$1 \times 10^{-5} \text{ m}$
e_u^d of the disk 2 and disk 3	0
e_v^d of the disk 1, disk 2, and disk 3	0
The coefficients of the bearings	
K_{xx}, K_{yy}	$1 \times 10^7 \text{ N/m}$
K_{xy}, K_{yx} (isotropic rotor-bearing system)	0
K_{xy}, K_{yx} (anisotropic rotor-bearing system)	$5 \times 10^6 \text{ N/m}$
$K_{\theta xx}, K_{\theta yy}, K_{\theta xy}, K_{\theta yx}$	0
K_ϕ of the left bearing	$3 \times 10^4 \text{ Nm/rad}$
K_ϕ of the right bearing	0
C_{xx}, C_{yy}	$2 \times 10^3 \text{ N s/m}$
$C_{xy}, C_{yx}, C_{\theta xx}, C_{\theta yy}, C_{\theta xy}, C_{\theta yx}$	0
C_ϕ of the left bearing	1 Nm s/rad
C_ϕ of the right bearing	0

a $1 \times$ torsional mode at 2516.7 rev/min. Fig. 11 illustrates the orbits of $1 \times$, $2 \times$, and synthetic whirls. The orbits of the $1 \times$ and $2 \times$ components are all forward, so that the synthetic orbit is also forward. At the rotating speed of 3050 rev/min (near the lateral resonant frequency), the amplitude of $1 \times$ whirl component exceeds that of the $2 \times$ whirl, and therefore the resulting synchronous orbit is right circular.

When $1 \times$ external torques are replaced by $2 \times$ ones, the nonsynchronous resonant peaks are located at 995.3 and 1258.0 rev/min, but the synchronous resonant peak is still located at 3022.6 rev/min (see Fig. 12). The positions of the resonant peaks are also irrelevant to the amplitude of the external torque. The whirling orbits at $T = 5000 \cos 2\Omega t \text{ Nm}$ are also displayed in Fig. 12. The response amplitudes and the whirling orbits of the components comprise $1 \times$ and $3 \times$ components, and are illustrated in Figs. 13 and 14, respectively. From Fig. 13, a $3 \times$ lateral mode occurs at 995.3 rev/min (around one-third of the lateral resonant frequency 3022.6 rev/min) since, under the system coupling effect, the $2 \times$ torque excites the $3 \times$ forward and $1 \times$ backward whirls. Furthermore, a $2 \times$ torsional mode occurs at 1258.0 rev/min (half of the torsional resonant frequency 2516.7 rev/min) and, because of the system coupling effect, these modes appear on the $1 \times$ and $3 \times$ whirl components simultaneously. The unbalance force excites the $1 \times$ forward

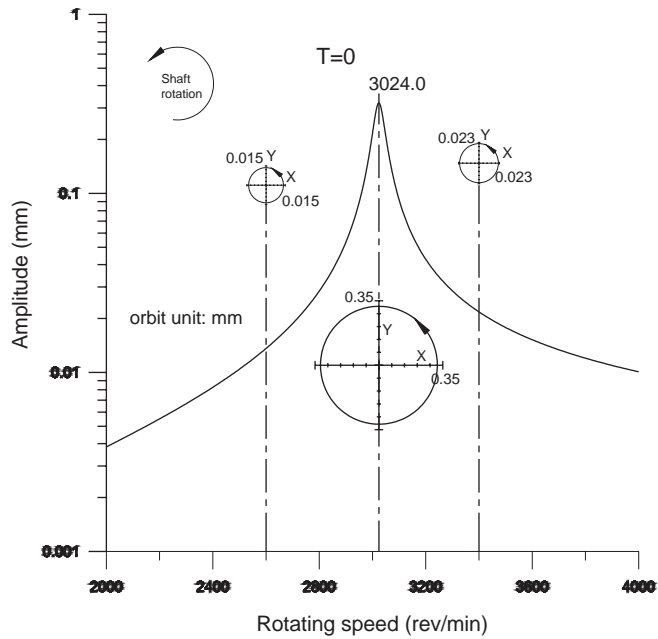


Fig. 8. Synchronous whirling orbits of disk 1 (isotropic rotor-bearing system without torque).

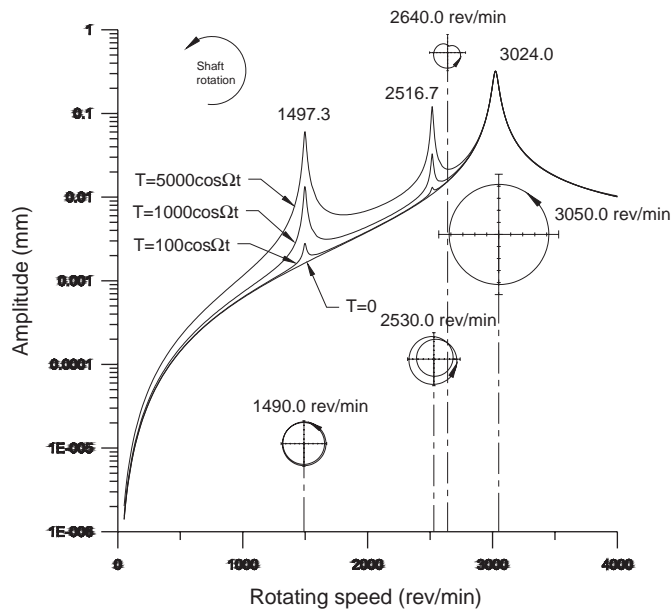


Fig. 9. Response amplitudes and orbits ($T = 5000 \cos \Omega t$) of disk 1 (isotropic rotor-bearing system with $1 \times$ torques).

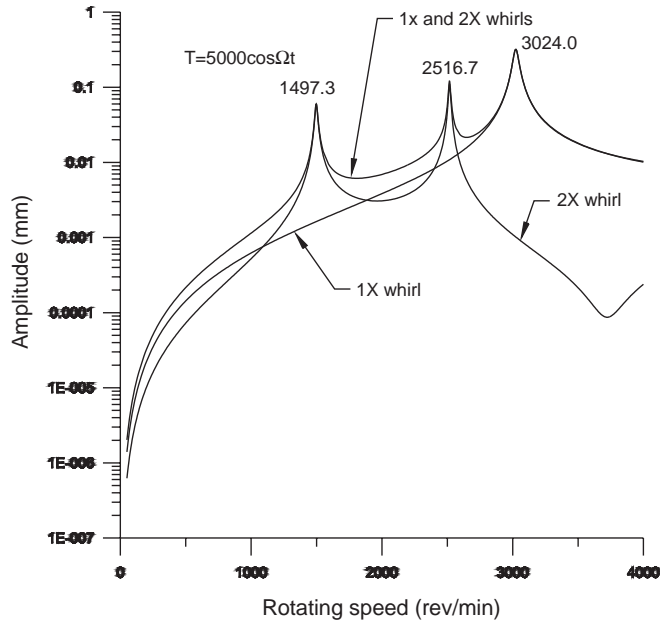


Fig. 10. Response amplitudes of the components of disk 1 (isotropic rotor-bearing system, $T = 5000 \cos \Omega t$).

component. The $1\times$ forward (excited by the unbalance force) and backward components (excited by the torque) may result in the $1\times$ ellipse whirl orbit. If the $1\times$ forward component is exceeding the backward component, the $1\times$ whirl orbit is forward, and vice versa. Finally, the $3\times$ whirl orbit, which is excited by the torque alone, is forward and right circular (see Fig. 14).

Fig. 15 shows the response amplitude and whirling orbits at $T = 5000 \cos 3\Omega t$ Nm. The response amplitudes and whirling orbits of the components are illustrated in Figs. 16 and 17 respectively. Fig. 16 indicates that the response components involve the $1\times$, $2\times$, and $4\times$ whirl. The response components of $2\times$ and $4\times$ whirls are excited by the external torque. A $2\times$ lateral mode appears at 1468.6 rev/min, and a $4\times$ lateral mode appears at 745.3 rev/min. $3\times$ torsional modes appear at 838.6 and 3712 rev/min and, due to the system coupling effect, these modes appear on the $2\times$ and $4\times$ whirl components simultaneously. The unbalance force excites the forward $1\times$ whirl and the torque excites the backward $2\times$ and forward $4\times$ whirls (see Fig. 17). At rotating speed of 3698 rev/min (near the second torsional mode), the amounts of the components are comparable, and thus the synthetic whirling orbit becomes complex.

As shown in Figs. 18–20, respectively, when the system is simultaneously excited by $1\times$, $2\times$, and $3\times$ external torque ($T = T_a(\cos \Omega t + \cos 2\Omega t + \cos 3\Omega t)$ Nm), the response amplitude, response amplitude of components, and whirl orbits are the sum of those when the system is excited by just one of these external torques. Table 2 lists the relations between the critical speeds and exciting frequency.

Case 2: Anisotropic rotor-bearing system: Fig. 21 shows the response amplitudes and orbits at $T = 0$ and $T = 1000 \cos \Omega t$ Nm when neglecting the eccentricity of the shaft. The response and

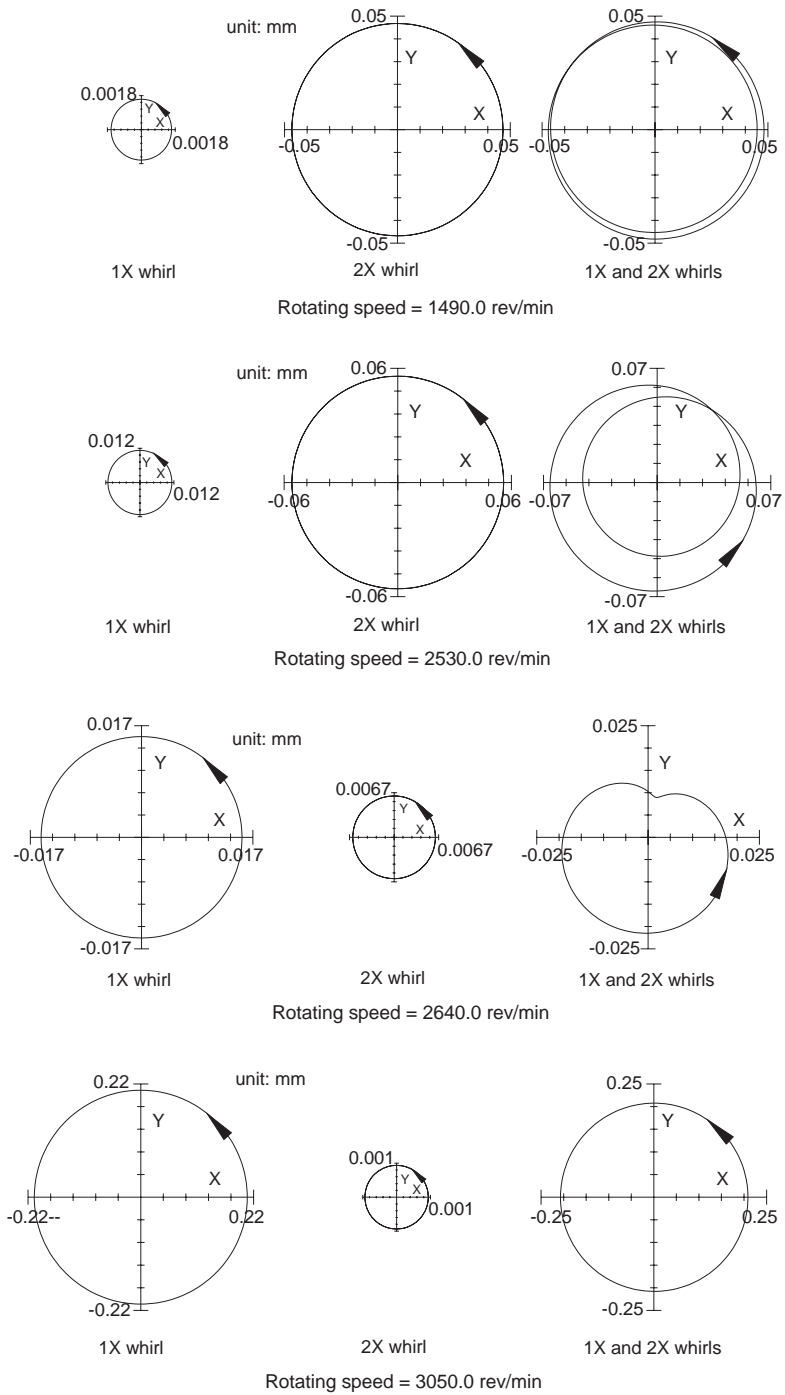


Fig. 11. Whirling orbits of disk 1 (isotropic rotor-bearing system, $T = 5000 \cos \Omega t$).

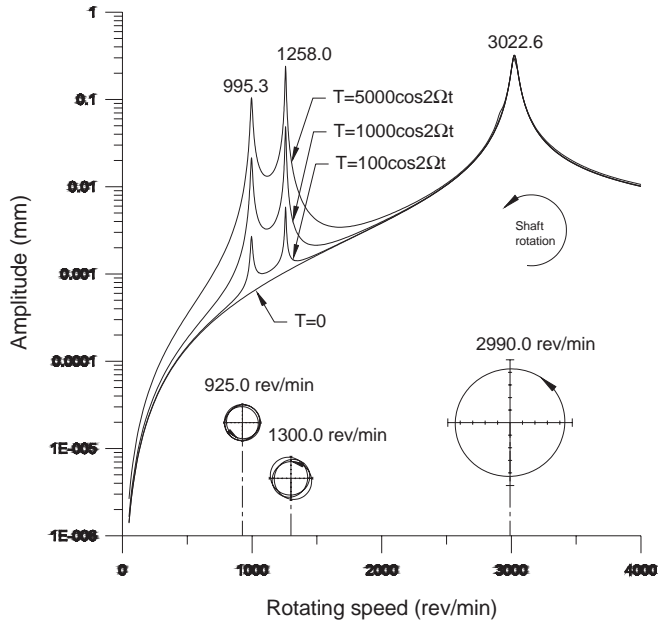


Fig. 12. Response amplitudes and orbits ($T = 5000 \cos 2\Omega t$) of disk 1 (isotropic rotor-bearing system with $2\times$ torques).

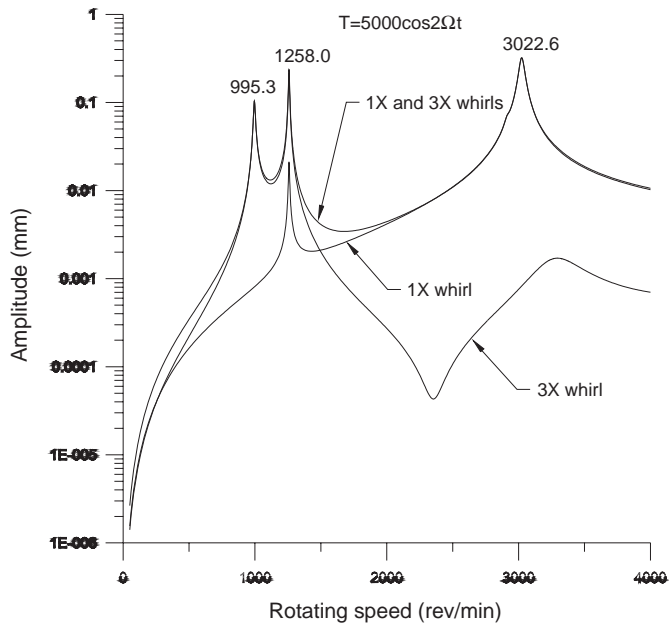


Fig. 13. Response amplitudes of the components of disk 1 (isotropic rotor-bearing system, $T = 5000 \cos 2\Omega t$).

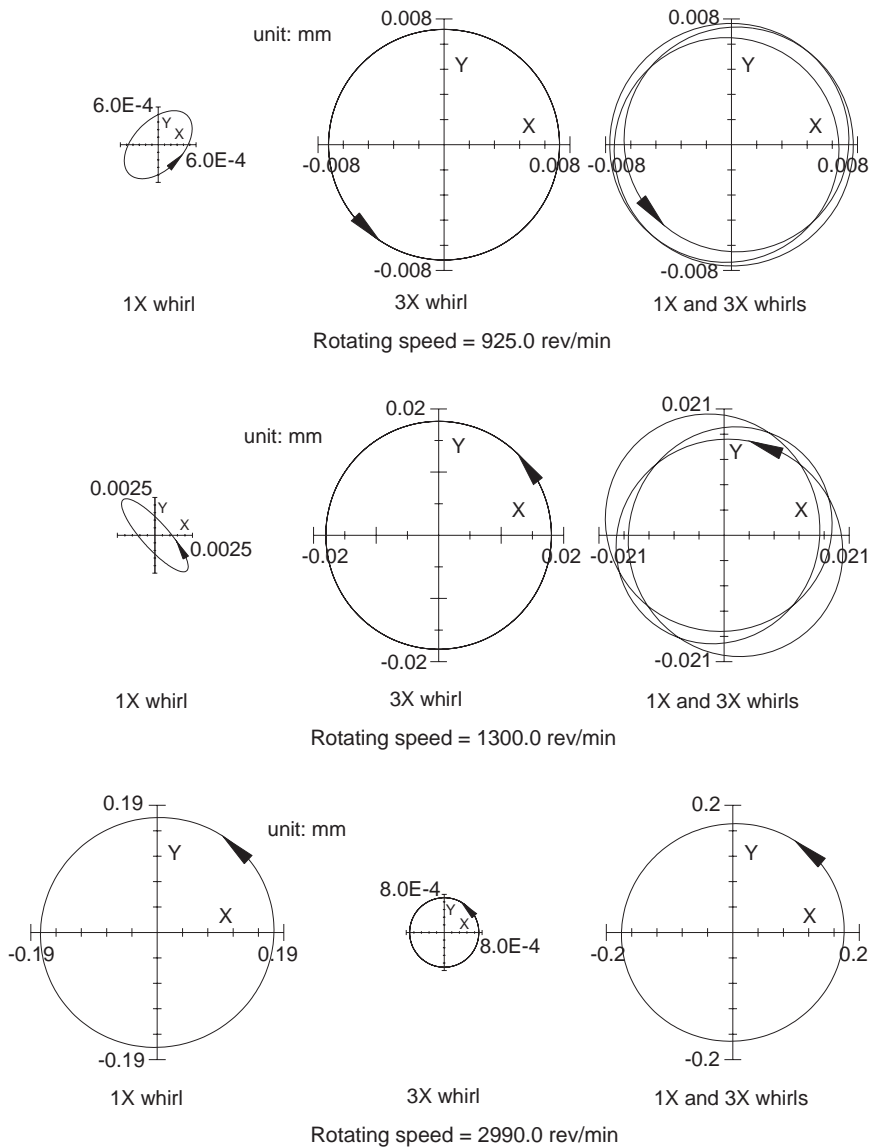


Fig. 14. Whirling orbits of disk 1 (isotropic rotor-bearing system, $T = 5000 \cos 2\Omega t$).

orbits at $T = 0$ are denoted by solid lines agree with our previous work of Lee et al. [19]. The analytical results reveals that, due to anisotropic bearing, two synchronous ($1\times$) lateral modes (2683.3 and 3082.6 rev/min) are excited and the orbits are always elliptical and synchronous for different rotating speeds. The synchronous whirling orbit reverses and becomes backward at speeds between the split critical speeds. The response and whirling orbit at $T = 1000 \cos \Omega t$ Nm are denoted by dashed lines. Besides the synchronous lateral modes, the external torque excites

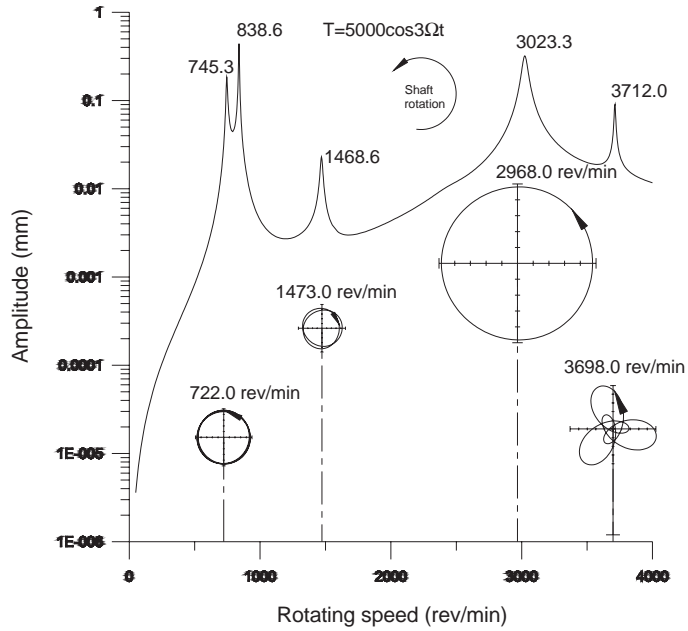


Fig. 15. Response amplitude and orbits of disk 1 (isotropic rotor-bearing system, $T = 5000 \cos 3\Omega t$).

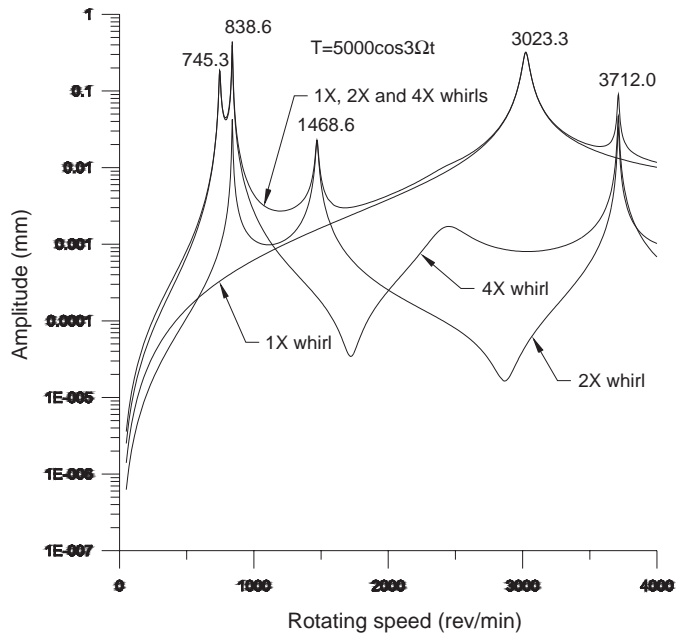


Fig. 16. Response amplitudes of the components of disk 1 (isotropic rotor-bearing system, $T = 5000 \cos 3\Omega t$).

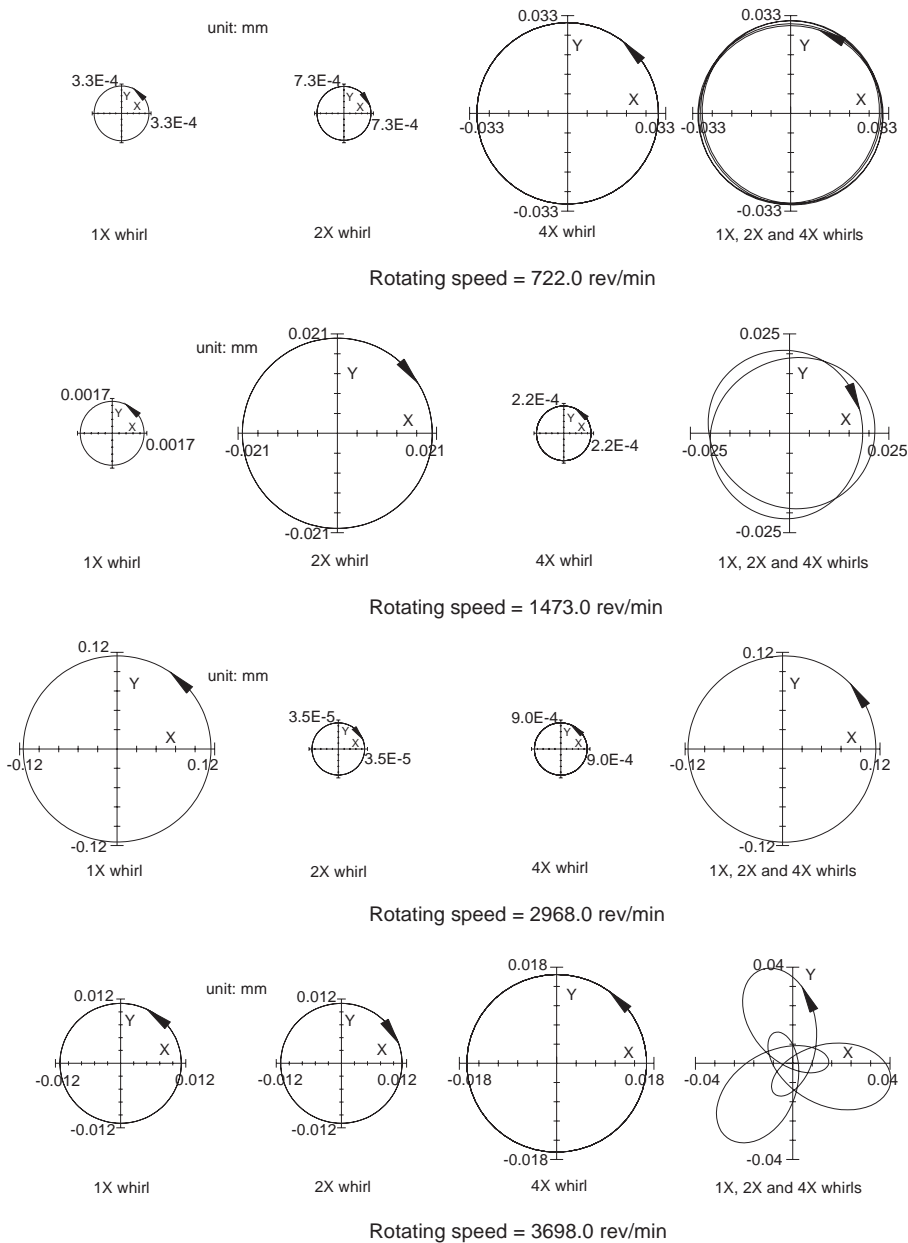


Fig. 17. Whirling orbits of disk 1 (isotropic rotor-bearing system, $T = 5000 \cos 3\Omega t$).

nonsynchronous ($2\times$) lateral modes (1344 and 1539.3 rev/min) and the torsional mode (2516 rev/min), which make the orbits no longer elliptical and synchronous. Consequently, the coupling effect is disregarded and the nonsynchronous lateral modes are left out when the lateral and torsional vibration are analyzed separately.

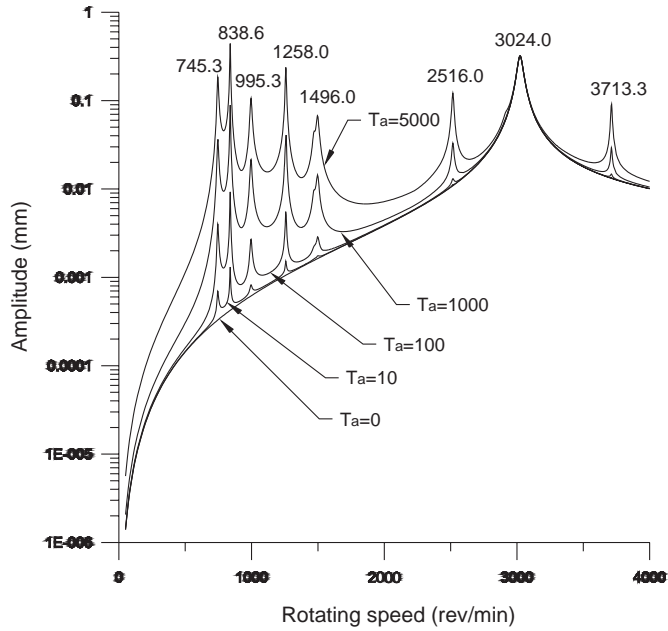


Fig. 18. Response amplitudes of disk 1 (isotropic rotor-bearing system with different torques).

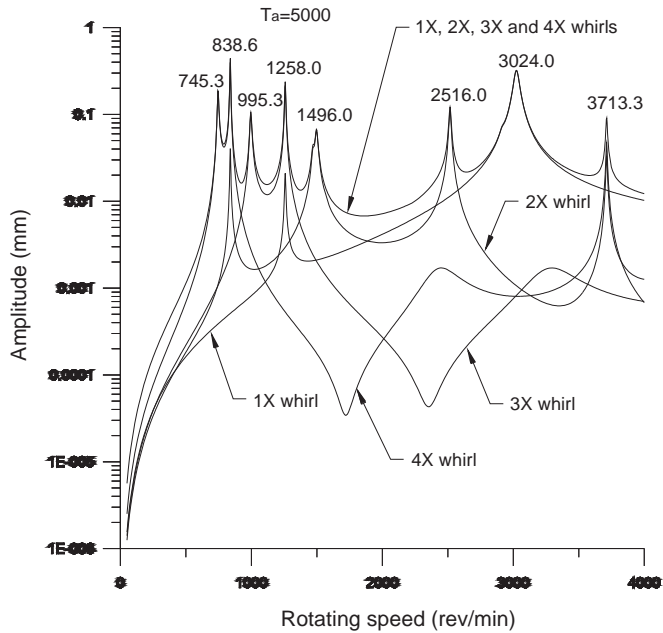


Fig. 19. Response amplitudes of the components of disk 1 (isotropic rotor-bearing system, $T_a = 5000$).

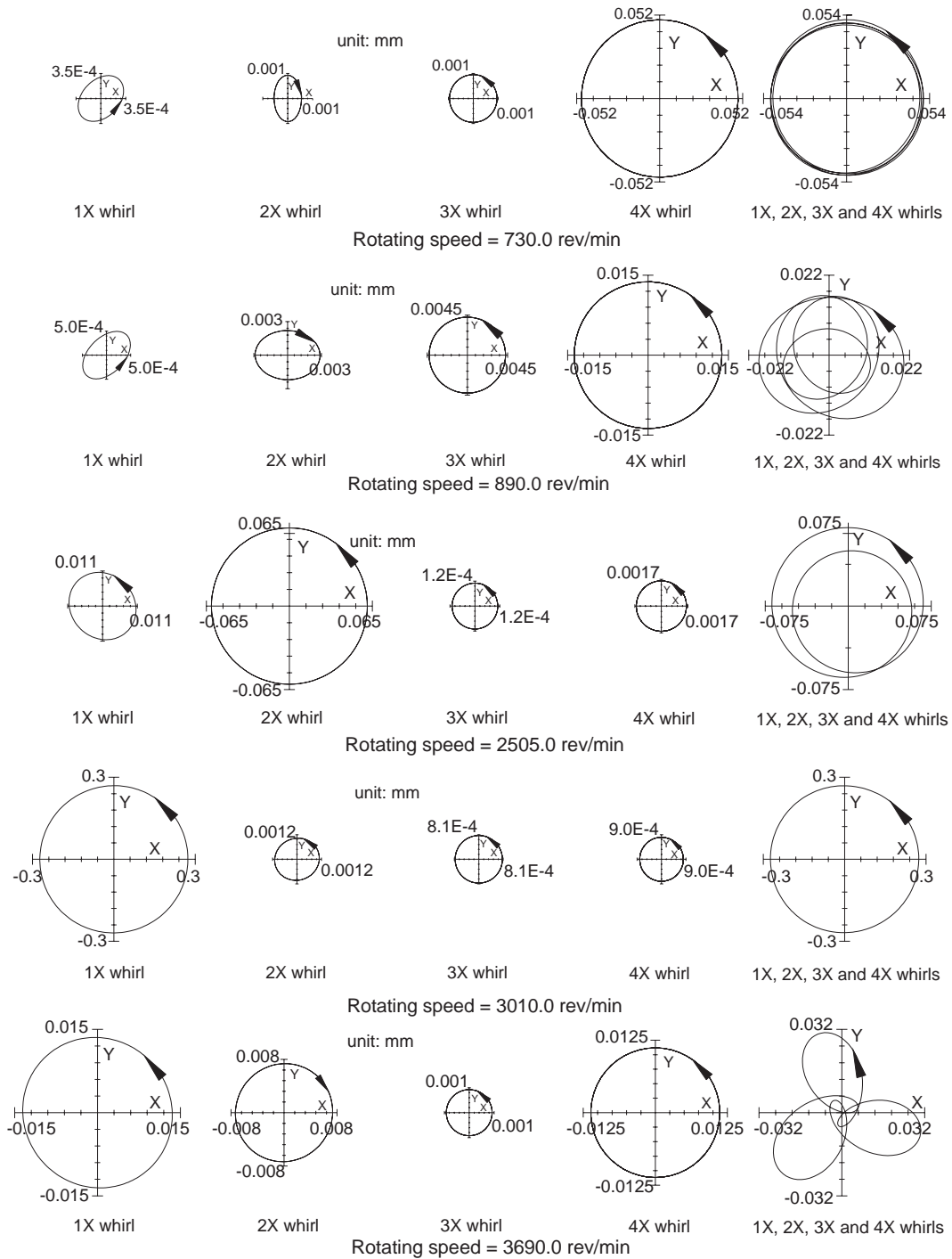


Fig. 20. Whirling orbits of disk 1 (isotropic rotor-bearing system, $T_a = 5000$).

Table 2
Critical speeds of the isotropic rotor-bearing system

External torque T (Nm)	Lateral natural frequency					
	The first mode (rev/min)					
	4× subcritical speed	3× subcritical speed	2× subcritical speed	(1×) synchronous critical speed		
A. Critical speeds corresponding to the lateral natural frequency						
$T = 0$				3024.0 (F)		
$T = 5000 \cos \Omega t$			1497.3 (F)	3024.0 (F)		
$T = 5000 \cos 2\Omega t$		995.3 (F)		3022.6 (F)		
$T = 5000 \cos 3\Omega t$	745.3 (F)		1468.6 (B)	3023.3 (F)		
$T = 5000(\cos \Omega t + \cos 2\Omega t + \cos 3\Omega t)$	745.3 (F)	995.3 (F)	1496.0 (F)	3024.0 (F)		
External torque T (Nm)	Torsional natural frequency					
	The first mode (rev/min)			The second mode (rev/min)		
	3× subcritical speed	2× subcritical speed	(1×) critical speed	3× subcritical speed	2× subcritical speed	(1×) critical speed
B. Critical speeds corresponding to the torsional natural frequency						
$T = 0$						
$T = 5000 \cos \Omega t$			2516.7			
$T = 5000 \cos 2\Omega t$		1258.0				
$T = 5000 \cos 3\Omega t$	838.6			3712.0		
$T = 5000(\cos \Omega t + \cos 2\Omega t + \cos 3\Omega t)$	838.6	1258.0	2516.0	3713.3		

F: forward, B: backward

Figs. 22–24 show the response amplitudes, component amplitudes, and whirl orbits at $T = T_a(\cos \Omega t + \cos 2\Omega t)$, respectively. Fig. 22 reveals that the synchronous resonance occurs at 3082 and 2682.6 rev/min. The steady response is comprised of the 1×, 2×, and 3× whirl components (Fig. 23). Because of the effect of the system coupling, two 2× lateral modes occur at 1538.6 and 1340 rev/min, two 3× lateral modes exist at 1025.3 and 897.3 rev/min, one 1× torsional mode occurs at 2517.3 rev/min, and one 2× torsional mode exists at 1258.0 rev/min.

Fig. 24 shows the orbit shapes of the 1×, 2×, and 3× whirls and the synthetic whirling orbit shape. The synthetic whirling orbit is complex because the whirl components involve the 1×, 2×, and 4× whirls. Table 3 lists the relations between the resonant critical speeds of the anisotropic rotor-bearing system and the exciting frequency.

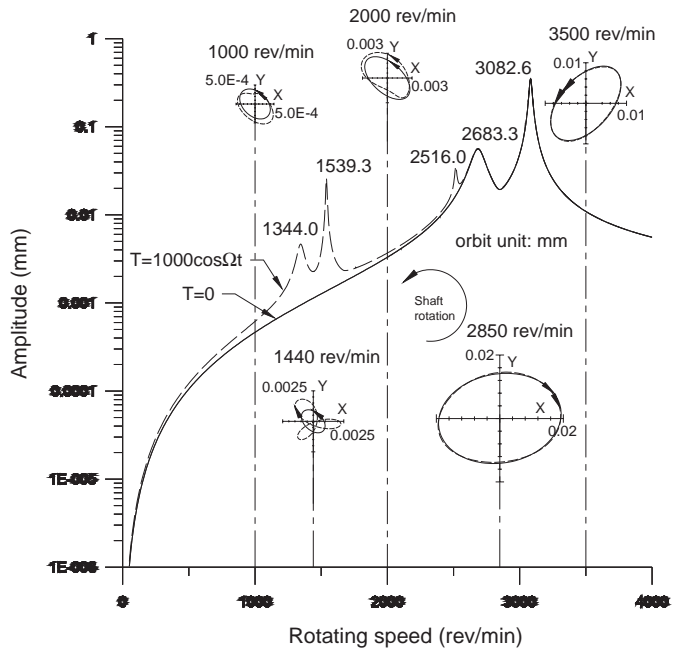


Fig. 21. Response amplitudes and orbits of disk 1 (anisotropic rotor-bearing system).

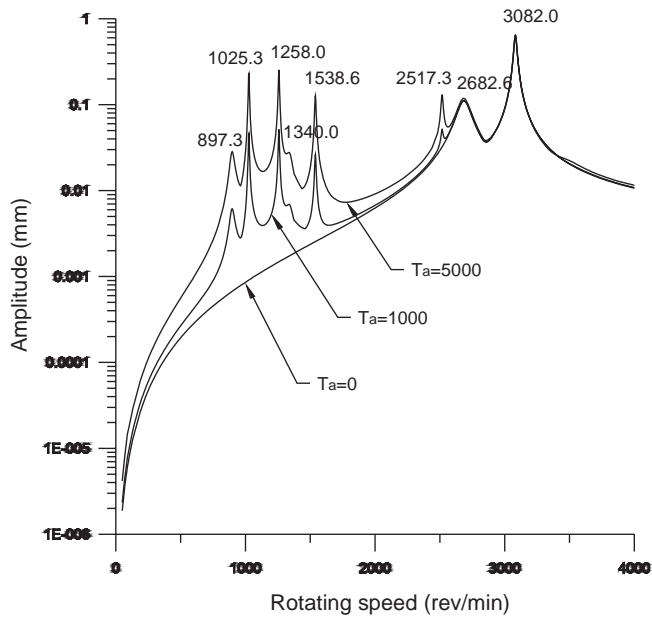


Fig. 22. Response amplitudes of disk 1 (anisotropic rotor-bearing system with different torques).

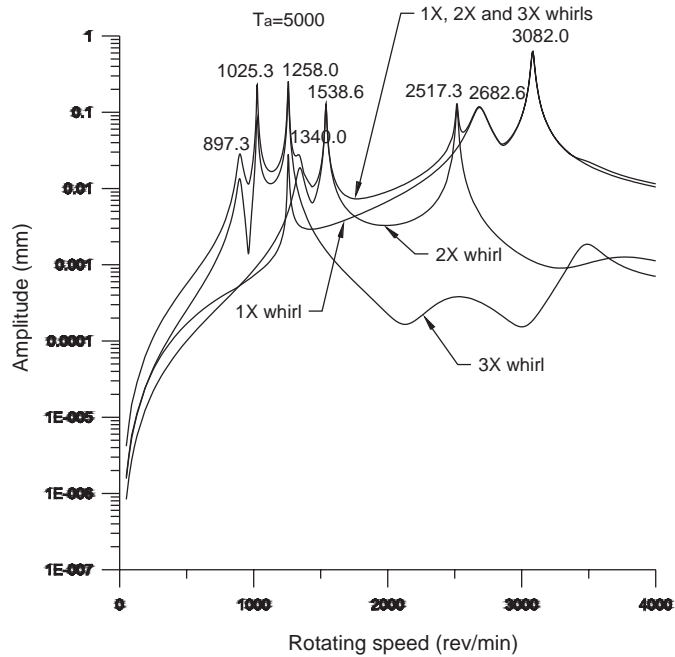


Fig. 23. Response amplitudes of the components of disk 1 (anisotropic rotor-bearing system, $T_a = 5000$).

8. Conclusion

The main objective of this work is to offer a modified TMM for analyzing the coupling lateral and torsional vibrations of the symmetric rotor-bearing systems with an external torque. The state variables of the modified transfer matrix include the lateral deflection, angular displacements, angle of twist, shear force, bending moment, and torque. The modified transfer matrix can be used to determine the steady-state responses of synchronous and superharmonic whirls of the coupling lateral and torsional vibrations. When the unbalance force alone excites the isotropic bearing-rotor system, the whirl orbit is synchronous, forward, and right circular, and only $1 \times$ lateral mode can be excited. However, when the unbalance force and the torque with $n \times$ frequency of the rotating speed excite the system simultaneously, the $(n + 1) \times$ forward and $(n - 1) \times$ backward whirls appear along with synchronous whirl. If the unbalance force alone excites the anisotropic bearing-rotor system, the whirl orbit is synchronous and elliptical. Two split $1 \times$ lateral modes appear and the synchronous whirl reverses direction and becomes backward between the split critical speeds. Like the isotropic system, if the unbalance force and the torque with $n \times$ frequency of the rotating speed excite the system simultaneously, the $(n + 1) \times$ and $(n - 1) \times$ whirls appear along with synchronous whirl. In conclusion, the external torque excites the superharmonic response and affects the dynamic behavior of the rotor-bearing system. Thus, during the design stage, the effect of the external torque should be considered carefully to avoid unexpectedly damaging the rotor-bearing system.

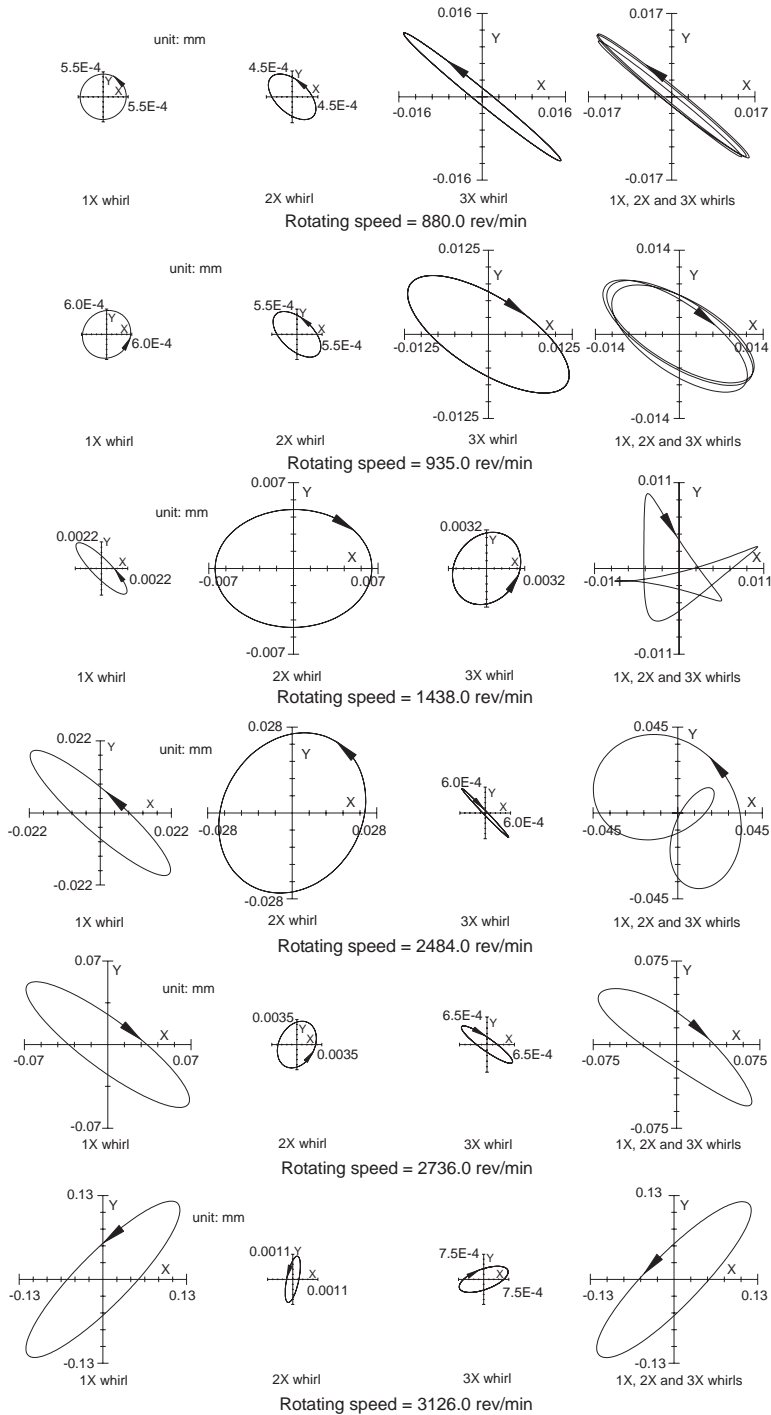


Fig. 24. Whirling orbits of disk 1 (anisotropic rotor-bearing system, $T_a = 5000$).

Table 3
Critical speeds of the anisotropic rotor-bearing system

External torque T (Nm)	Lateral natural frequency		
	The first mode (rev/min)		
	3× subcritical speed	2× subcritical speed	(1×) synchronous critical speed
A. Critical speeds corresponding to the lateral natural frequency			
$T = 0$			2683.3 (B) 3082.6 (F)
$T = 1000 \cos \Omega t$		1344.0 (B) 1539.3 (F)	2683.3(B) 3082.6 (F)
$T = 5000(\cos \Omega t + \cos 2\Omega t)$	897.3 (B) 1025.3 (F)	1340.0 (B) 1538.6 (F)	2682.6 (B) 3082.0 (F)
External torque T (Nm)	Torsional natural frequency		
	The first mode (rev/min)		
	2× subcritical speed		(1×) critical speed
B. Critical speeds corresponding to the torsional natural frequency			
$T = 0$			
$T = 1000 \cos \Omega t$			2516.0
$T = 5000(\cos \Omega t + \cos 2\Omega t)$		1258.0	2517.3

F: forward, B: backward

Acknowledgement

The authors would like to thank the National Science Council of the Republic of China, Taiwan for financially supporting this research under Contract No. NSC 92-2212-E-009-020.

Appendix A

Substituting Eq. (28) into Eqs. (22)–(26) and equating coefficients of the same harmonic terms, the following equations are obtained:

$$k_s G A x_0'' - k_s G A \theta_{y,0}' = 0, \quad (\text{A.1})$$

$$\begin{aligned} k_s G A x_{1c}'' - k_s G A \theta_{y,1c}' + \rho A \Omega^2 x_{1c} - \frac{1}{2} \rho A e_v^s \Omega^2 \varphi_{2c} - \frac{1}{2} \rho A e_u^s \Omega^2 \varphi_{2s} - \rho A \Omega^2 e_v^s \varphi_0 \\ = -\rho A \Omega^2 e_u^s, \end{aligned} \quad (\text{A.2})$$

$$\begin{aligned} k_s G A x''_{1s} - k_s G A \theta'_{y,1s} + \rho A \Omega^2 x_{1s} - \frac{1}{2} \rho A e_v^s \Omega^2 \varphi_{2s} + \frac{1}{2} \rho A e_u^s \Omega^2 \varphi_{2c} - \rho A \Omega^2 e_u^s \varphi_0 \\ = \rho A \Omega^2 e_v^s, \end{aligned} \quad (\text{A.3})$$

$$\begin{aligned} k_s G A x''_{2c} - k_s G A \theta'_{y,2c} + \rho A 4 \Omega^2 x_{2c} - 2 \rho A e_v^s \Omega^2 \varphi_{3c} - 2 \rho A e_u^s \Omega^2 \varphi_{3s} - 2 \rho A e_v^s \Omega^2 \varphi_{1c} \\ + 2 \rho A e_u^s \Omega^2 \varphi_{1s} = 0, \end{aligned} \quad (\text{A.4})$$

$$\begin{aligned} k_s G A x''_{2s} - k_s G A \theta'_{y,2s} + \rho A 4 \Omega^2 x_{2s} - 2 \rho A e_v^s \Omega^2 \varphi_{3s} + 2 \rho A e_u^s \Omega^2 \varphi_{3c} - 2 \rho A e_v^s \Omega^2 \varphi_{1s} \\ - 2 \rho A e_u^s \Omega^2 \varphi_{1c} = 0, \end{aligned} \quad (\text{A.5})$$

$$\begin{aligned} k_s G A x''_{jc} - k_s G A \theta'_{y,jc} + \rho A j^2 \Omega^2 x_{jc} - \frac{1}{2} \rho A e_v^s j^2 \Omega^2 \varphi_{(j+1)c} - \frac{1}{2} \rho A e_u^s j^2 \Omega^2 \varphi_{(j+1)s} \\ - \frac{1}{2} \rho A e_v^s j^2 \Omega^2 \varphi_{(j-1)c} + \frac{1}{2} \rho A e_u^s j^2 \Omega^2 \varphi_{(j-1)s} = 0, \end{aligned} \quad (\text{A.6})$$

$$\begin{aligned} k_s G A x''_{js} - k_s G A \theta'_{y,js} + \rho A j^2 \Omega^2 x_{js} - \frac{1}{2} \rho A e_v^s j^2 \Omega^2 \varphi_{(j+1)s} + \frac{1}{2} \rho A e_u^s j^2 \Omega^2 \varphi_{(j+1)c} \\ - \frac{1}{2} \rho A e_v^s j^2 \Omega^2 \varphi_{(j-1)s} - \frac{1}{2} \rho A e_u^s j^2 \Omega^2 \varphi_{(j-1)c} = 0, \end{aligned} \quad (\text{A.7})$$

$$k_s G A x''_{nc} - k_s G A \theta'_{y,nc} + \rho A n^2 \Omega^2 x_{nc} - \frac{1}{2} \rho A e_v^s n^2 \Omega^2 \varphi_{(n-1)c} + \frac{1}{2} \rho A e_u^s n^2 \Omega^2 \varphi_{(n-1)s} = 0, \quad (\text{A.8})$$

$$k_s G A x''_{ns} - k_s G A \theta'_{y,ns} + \rho A n^2 \Omega^2 x_{ns} - \frac{1}{2} \rho A e_v^s n^2 \Omega^2 \varphi_{(n-1)s} - \frac{1}{2} \rho A e_u^s n^2 \Omega^2 \varphi_{(n-1)c} = 0, \quad (\text{A.9})$$

$$k_s G A \theta'_{x,0} + k_s G A y''_0 = \rho A g, \quad (\text{A.10})$$

$$\begin{aligned} k_s G A \theta'_{x,1c} + k_s G A y''_{1c} + \rho A \Omega^2 y_{1c} + \frac{1}{2} \rho A e_u^s \Omega^2 \varphi_{2c} - \frac{1}{2} \rho A e_v^s \Omega^2 \varphi_{2s} + \rho A \Omega^2 e_u^s \varphi_0 \\ = -\rho A \Omega^2 e_v^s, \end{aligned} \quad (\text{A.11})$$

$$\begin{aligned} k_s G A \theta'_{x,1s} + k_s G A y''_{1s} + \rho A \Omega^2 y_{1s} + \frac{1}{2} \rho A e_u^s \Omega^2 \varphi_{2s} + \frac{1}{2} \rho A e_v^s \Omega^2 \varphi_{2c} - \rho A \Omega^2 e_v^s \varphi_0 \\ = -\rho A \Omega^2 e_u^s, \end{aligned} \quad (\text{A.12})$$

$$\begin{aligned} k_s G A \theta'_{x,2c} + k_s G A y''_{2c} + \rho A 4 \Omega^2 y_{2c} + 2 \rho A e_u^s \Omega^2 \varphi_{3c} - 2 \rho A e_v^s \Omega^2 \varphi_{3s} + 2 \rho A e_u^s \Omega^2 \varphi_{1c} \\ + 2 \rho A e_v^s \Omega^2 \varphi_{1s} = 0, \end{aligned} \quad (\text{A.13})$$

$$\begin{aligned} k_s G A \theta'_{x,2s} + k_s G A y''_{2s} + \rho A 4 \Omega^2 y_{2s} + 2 \rho A e_u^s \Omega^2 \varphi_{3s} + 2 \rho A e_v^s \Omega^2 \varphi_{3c} + 2 \rho A e_u^s \Omega^2 \varphi_{1s} \\ - 2 \rho A e_v^s \Omega^2 \varphi_{1c} = 0, \end{aligned} \quad (\text{A.14})$$

$$\begin{aligned} k_s G A \theta'_{x,jc} + k_s G A y''_{jc} + \rho A j^2 \Omega^2 y_{jc} + \frac{1}{2} \rho A e_u^s j^2 \Omega^2 \varphi_{(j+1)c} - \frac{1}{2} \rho A e_v^s j^2 \Omega^2 \varphi_{(j+1)s} \\ + \frac{1}{2} \rho A e_u^s j^2 \Omega^2 \varphi_{(j-1)c} + \frac{1}{2} \rho A e_v^s j^2 \Omega^2 \varphi_{(j-1)s} = 0, \end{aligned} \quad (\text{A.15})$$

$$\begin{aligned} k_s G A \theta'_{x,js} + k_s G A y''_{js} + \rho A j^2 \Omega^2 y_{js} + \frac{1}{2} \rho A e_u^s j^2 \Omega^2 \varphi_{(j+1)s} + \frac{1}{2} \rho A e_v^s j^2 \Omega^2 \varphi_{(j+1)c} \\ + \frac{1}{2} \rho A e_u^s j^2 \Omega^2 \varphi_{(j-1)s} - \frac{1}{2} \rho A e_v^s j^2 \Omega^2 \varphi_{(j-1)c} = 0, \end{aligned} \quad (\text{A.16})$$

$$k_s GA\theta'_{x,nc} + k_s GAy''_{nc} + \rho An^2 \Omega^2 y_{nc} + \frac{1}{2} \rho Ae_u^s n^2 \Omega^2 \varphi_{(n-1)c} + \frac{1}{2} \rho Ae_v^s n^2 \Omega^2 \varphi_{(n-1)s} = 0, \quad (\text{A.17})$$

$$k_s GA\theta'_{x,ns} + k_s GAy''_{ns} + \rho An^2 \Omega^2 y_{ns} + \frac{1}{2} \rho Ae_u^s n^2 \Omega^2 \varphi_{(n-1)s} - \frac{1}{2} \rho Ae_v^s n^2 \Omega^2 \varphi_{(n-1)c} = 0, \quad (\text{A.18})$$

$$EI^s \theta''_{x,0} - k_s GA\theta_{x,0} - k_s GAy'_0 = 0, \quad (\text{A.19})$$

$$EI^s \theta''_{x,ic} - k_s GA\theta_{x,ic} - k_s GAy'_{ic} - \rho I_p^s \Omega i \Omega \theta_{y,is} + \rho I^s i^2 \Omega^2 \theta_{x,ic} = 0, \quad (\text{A.20})$$

$$EI^s \theta''_{x,is} - k_s GA\theta_{x,is} - k_s GAy'_{is} + \rho I_p^s \Omega i \Omega \theta_{y,ic} + \rho I^s i^2 \Omega^2 \theta_{x,is} = 0, \quad (\text{A.21})$$

$$-EI^s \theta''_{y,0} - k_s GAx'_0 + k_s GA\theta_{y,0} = 0, \quad (\text{A.22})$$

$$-EI^s \theta''_{y,ic} - k_s GAx'_{ic} + k_s GA\theta_{y,ic} - \rho I_p^s \Omega i \Omega \theta_{x,is} - \rho I^s i^2 \Omega^2 \theta_{y,ic} = 0, \quad (\text{A.23})$$

$$-EI^s \theta''_{y,is} - k_s GAx'_{is} + k_s GA\theta_{y,is} + \rho I_p^s \Omega i \Omega \theta_{x,ic} - \rho I^s i^2 \Omega^2 \theta_{y,is} = 0, \quad (\text{A.24})$$

$$GI_p^s \varphi''_0 - \frac{1}{2} \rho Ae_v^s \Omega^2 x_{1c} - \frac{1}{2} \rho Ae_u^s \Omega^2 x_{1s} + \frac{1}{2} \rho Ae_u^s \Omega^2 y_{1c} - \frac{1}{2} \rho Ae_v^s \Omega^2 y_{1s} = 0, \quad (\text{A.25})$$

$$GI_p^s \varphi''_{1c} + \rho A(e^s)^2 \Omega^2 \varphi_{1c} + \rho I_p^s \Omega^2 \varphi_{1c} - 2\rho Ae_v^s \Omega^2 x_{2c} - 2\rho Ae_u^s \Omega^2 x_{2s} + 2\rho Ae_u^s \Omega^2 y_{2c} - 2\rho Ae_v^s \Omega^2 y_{2s} = 0, \quad (\text{A.26})$$

$$GI_p^s \varphi''_{1s} + \rho A(e^s)^2 \Omega^2 \varphi_{1s} + \rho I_p^s \Omega^2 \varphi_{1s} - 2\rho Ae_v^s \Omega^2 x_{2s} + 2\rho Ae_u^s \Omega^2 x_{2c} + 2\rho Ae_u^s \Omega^2 y_{2s} + 2\rho Ae_v^s \Omega^2 y_{2c} = 0, \quad (\text{A.27})$$

$$\begin{aligned} & -\frac{1}{2} \rho Ae_v^s \Omega^2 x_{1c} + \frac{1}{2} \rho Ae_u^s \Omega^2 x_{1s} + \frac{1}{2} \rho Ae_u^s \Omega^2 y_{1c} + \frac{1}{2} \rho Ae_v^s \Omega^2 y_{1s} + GI_p^s \varphi''_{2c} \\ & + 4\rho A(e^s)^2 \Omega^2 \varphi_{2c} + 4\rho I_p^s \Omega^2 \varphi_{2c} - \rho Ae_v^s \frac{9}{2} \Omega^2 x_{3c} - \rho Ae_u^s \frac{9}{2} \Omega^2 x_{3s} \\ & + \rho Ae_u^s \frac{9}{2} \Omega^2 y_{3c} - \rho Ae_v^s \frac{9}{2} \Omega^2 y_{3s} = 0, \end{aligned} \quad (\text{A.28})$$

$$\begin{aligned} & -\frac{1}{2} \rho Ae_v^s \Omega^2 x_{1s} - \frac{1}{2} \rho Ae_u^s \Omega^2 x_{1c} + \frac{1}{2} \rho Ae_u^s \Omega^2 y_{1s} - \frac{1}{2} \rho Ae_v^s \Omega^2 y_{1c} + GI_p^s \varphi''_{2s} \\ & + 4\rho A(e^s)^2 \Omega^2 \varphi_{2s} + 4\rho I_p^s \Omega^2 \varphi_{2s} - \rho Ae_v^s \frac{9}{2} \Omega^2 x_{3s} + \rho Ae_u^s \frac{9}{2} \Omega^2 x_{3c} \\ & + \rho Ae_u^s \frac{9}{2} \Omega^2 y_{3s} + \rho Ae_v^s \frac{9}{2} \Omega^2 y_{3c} = 0, \end{aligned} \quad (\text{A.29})$$

$$\begin{aligned} & GI_p^s \varphi''_{jc} + j^2 \rho A(e^s)^2 \Omega^2 \varphi_{jc} + j^2 \rho I_p^s \Omega^2 \varphi_{jc} - \rho Ae_v^s (j+1)^2 \frac{1}{2} \Omega^2 x_{(j+1)c} \\ & - \rho Ae_v^s (j-1)^2 \frac{1}{2} \Omega^2 x_{(j-1)c} - \rho Ae_u^s (j+1)^2 \frac{1}{2} \Omega^2 x_{(j+1)s} + \rho Ae_u^s (j-1)^2 \frac{1}{2} \Omega^2 x_{(j-1)s} + \rho Ae_u^s (j+1)^2 \frac{1}{2} \Omega^2 y_{(j+1)c} \\ & + \rho Ae_u^s (j-1)^2 \frac{1}{2} \Omega^2 y_{(j-1)c} - \rho Ae_v^s (j+1)^2 \frac{1}{2} \Omega^2 y_{(j+1)s} + \rho Ae_v^s (j-1)^2 \frac{1}{2} \Omega^2 y_{(j-1)s} = 0, \end{aligned} \quad (\text{A.30})$$

$$\begin{aligned}
& GI_p^s \phi_{js}'' + j^2 \rho A (e^s)^2 \Omega^2 \phi_{js} + j^2 \rho I_p^s \Omega^2 \phi_{js} - \rho A e_v^s (j+1)^{\frac{21}{2}} \Omega^2 x_{(j+1)s} \\
& - \rho A e_v^s (j-1)^{\frac{21}{2}} \Omega^2 x_{(j-1)s} + \rho A e_u^s (j+1)^{\frac{21}{2}} \Omega^2 x_{(j+1)c} - \rho A e_u^s (j-1)^{\frac{21}{2}} \Omega^2 x_{(j-1)c} \\
& + \rho A e_u^s (j+1)^{\frac{21}{2}} \Omega^2 y_{(j+1)s} + \rho A e_u^s (j-1)^{\frac{21}{2}} \Omega^2 y_{(j-1)s} + \rho A e_v^s (j+1)^{\frac{21}{2}} \Omega^2 y_{(j+1)c} \\
& - \rho A e_v^s (j-1)^{\frac{21}{2}} \Omega^2 y_{(j-1)c} = 0,
\end{aligned} \tag{A.31}$$

$$\begin{aligned}
& GI_p^s \phi_{nc}'' + n^2 \rho A (e^s)^2 \Omega^2 \phi_{nc} + n^2 \rho I_p^s \Omega^2 \phi_{nc} - \rho A e_v^s (n-1)^{\frac{21}{2}} \Omega^2 x_{(n-1)c} \\
& + \rho A e_u^s (n-1)^{\frac{21}{2}} \Omega^2 x_{(n-1)s} + \rho A e_u^s (n-1)^{\frac{21}{2}} \Omega^2 y_{(n-1)c} \\
& + \rho A e_v^s (n-1)^{\frac{21}{2}} \Omega^2 y_{(n-1)s} = 0,
\end{aligned} \tag{A.32}$$

$$\begin{aligned}
& GI_p^s \phi_{ns}'' + n^2 \rho A (e^s)^2 \Omega^2 \phi_{ns} + n^2 \rho I_p^s \Omega^2 \phi_{ns} - \rho A e_v^s (n-1)^{\frac{21}{2}} \Omega^2 x_{(n-1)s} \\
& - \rho A e_u^s (n-1)^{\frac{21}{2}} \Omega^2 x_{(n-1)c} + \rho A e_u^s (n-1)^{\frac{21}{2}} \Omega^2 y_{(n-1)s} \\
& - \rho A e_v^s (n-1)^{\frac{21}{2}} \Omega^2 y_{(n-1)c} = 0,
\end{aligned} \tag{A.33}$$

where

$$i = 1, 2, 3, \dots, n, \text{ and } j = 3, 4, 5, \dots, n-1.$$

Appendix B

$$\begin{aligned}
\mathbf{E}_2(1, 1) &= \mathbf{E}_2(2, 2) = \mathbf{E}_2(2+n, 2+n) = \mathbf{E}_2(3, 3) = \mathbf{E}_2(3+n, 3+n) \\
&= \mathbf{E}_2(1+j, 1+j) = \mathbf{E}_2(1+n+j, 1+n+j) = \mathbf{E}_2(1+n, 1+n) \\
&= \mathbf{E}_2(1+2n, 1+2n) = \mathbf{E}_2(2+2n, 2+2n) \\
&= \mathbf{E}_2(3+2n, 3+2n) = \mathbf{E}_2(3+3n, 3+3n) = \mathbf{E}_2(4+2n, 4+2n) = \mathbf{E}_2(4+3n, 4+3n) \\
&= \mathbf{E}_2(2+2n+j, 2+2n+j) = \mathbf{E}_2(2+3n+j, 2+3n+j) = \mathbf{E}_2(2+3n, 2+3n) \\
&= \mathbf{E}_2(2+4n, 2+4n) = m,
\end{aligned}$$

$$\begin{aligned}
\mathbf{E}_2(3+4n, 3+4n) &= \mathbf{E}_2(3+4n+i, 3+4n+i) = \mathbf{E}_2(3+5n+i, 3+5n+i) \\
&= -\mathbf{E}_2(4+6n, 4+6n) = -\mathbf{E}_2(4+6n+i, 4+6n+i) \\
&= -\mathbf{E}_2(4+7n+i, 4+7n+i) = a,
\end{aligned}$$

$$\begin{aligned}
\mathbf{E}_2(5+8n, 5+8n) &= \mathbf{E}_2(6+8n, 6+8n) = \mathbf{E}_2(6+9n, 6+9n) = \mathbf{E}_2(7+8n, 7+8n) \\
&= \mathbf{E}_2(7+9n, 7+9n) = \mathbf{E}_2(5+8n+j, 5+8n+j) = \mathbf{E}_2(5+9n+j, 5+9n+j) \\
&= \mathbf{E}_2(5+9n, 5+9n) = \mathbf{E}_2(5+10n, 5+10n) = h,
\end{aligned}$$

$$\begin{aligned}
-\mathbf{E}_1(1, 4 + 6n) &= -\mathbf{E}_1(2, 5 + 6n) = -\mathbf{E}_1(2 + n, 5 + 7n) = -\mathbf{E}_1(3, 6 + 6n) = -\mathbf{E}_1(3 + n, 6 + 7n) \\
&= -\mathbf{E}_1(1 + j, 4 + 6n + j) = -\mathbf{E}_1(1 + n + j, 4 + 7n + j) \\
&= -\mathbf{E}_1(1 + n, 4 + 7n) = -\mathbf{E}_1(1 + 2n, 4 + 8n) = \mathbf{E}_1(2 + 2n, 3 + 4n) \\
&= \mathbf{E}_1(3 + 2n, 4 + 4n) = \mathbf{E}_1(3 + 3n, 4 + 5n) \\
&= \mathbf{E}_1(4 + 2n, 5 + 4n) = \mathbf{E}_1(4 + 3n, 5 + 5n) = \mathbf{E}_1(2 + 2n + j, 3 + 4n + j) \\
&= \mathbf{E}_1(2 + 3n + j, 3 + 5n + j) = \mathbf{E}_1(2 + 3n, 3 + 5n) = \mathbf{E}_1(2 + 4n, 3 + 6n) \\
&= -\mathbf{E}_1(3 + 4n, 2 + 2n) = -\mathbf{E}_1(3 + 4n + i, 2 + 2n + i) = -\mathbf{E}_1(3 + 5n + i, 2 + 3n + i) \\
&= -\mathbf{E}_1(4 + 6n, 1) = -\mathbf{E}_1(4 + 6n + i, 1 + i) = -\mathbf{E}_1(4 + 7n + i, 1 + n + i) = m,
\end{aligned}$$

$$-\mathbf{E}_0(3 + 4n, 3 + 4n) = \mathbf{E}_0(4 + 6n, 4 + 6n) = m,$$

$$\begin{aligned}
-\mathbf{E}_0(3 + 4n + i, 3 + 4n + i) &= -\mathbf{E}_0(3 + 5n + i, 3 + 5n + i) = \mathbf{E}_0(4 + 6n + i, 4 + 6n + i) \\
&= \mathbf{E}_0(4 + 7n + i, 4 + 7n + i) = m - i^2b,
\end{aligned}$$

$$\mathbf{E}_0(2, 2) = \mathbf{E}_0(2 + n, 2 + n) = \mathbf{E}_0(3 + 2n, 3 + 2n) = \mathbf{E}_0(3 + 3n, 3 + 3n) = c,$$

$$\mathbf{E}_0(3, 3) = \mathbf{E}_0(3 + n, 3 + n) = \mathbf{E}_0(4 + 2n, 4 + 2n) = \mathbf{E}_0(4 + 3n, 4 + 3n) = 4c,$$

$$\begin{aligned}
\mathbf{E}_0(1 + j, 1 + j) &= \mathbf{E}_0(1 + n + j, 1 + n + j) = \mathbf{E}_0(2 + 2n + j, 2 + 2n + j) \\
&= \mathbf{E}_0(2 + 3n + j, 2 + 3n + j) = j^2c,
\end{aligned}$$

$$\mathbf{E}_0(1 + n, 1 + n) = \mathbf{E}_0(1 + 2n, 1 + 2n) = \mathbf{E}_0(2 + 3n, 2 + 3n) = \mathbf{E}_0(2 + 4n, 2 + 4n) = n^2c,$$

$$\mathbf{E}_0(6 + 8n, 6 + 8n) = \mathbf{E}_0(6 + 9n, 6 + 9n) = s,$$

$$\mathbf{E}_0(7 + 8n, 7 + 8n) = \mathbf{E}_0(7 + 9n, 7 + 9n) = 4s,$$

$$\mathbf{E}_0(5 + 8n + j, 5 + 8n + j) = \mathbf{E}_0(5 + 9n + j, 5 + 9n + j) = j^2s,$$

$$\mathbf{E}_0(5 + 9n, 5 + 9n) = \mathbf{E}_0(5 + 10n, 5 + 10n) = n^2s,$$

$$\begin{aligned}
-\mathbf{E}_0(3 + 4n + i, 4 + 7n + i) &= \mathbf{E}_0(3 + 5n + i, 4 + 6n + i) = -\mathbf{E}_0(4 + 6n + i, 3 + 5n + i) \\
&= \mathbf{E}_0(4 + 7n + i, 3 + 4n + i) = id,
\end{aligned}$$

$$\begin{aligned}
-\mathbf{E}_0(2, 7 + 9n) &= \mathbf{E}_0(2 + n, 7 + 8n) = \mathbf{E}_0(3 + 2n, 7 + 8n) = \mathbf{E}_0(3 + 3n, 7 + 9n) \\
&= -\mathbf{E}_0(5 + 8n, 2 + n) = \mathbf{E}_0(5 + 8n, 3 + 2n) = \mathbf{E}_0(7 + 8n, 2 + n) \\
&= \mathbf{E}_0(7 + 8n, 3 + 2n) = -\mathbf{E}_0(7 + 9n, 2) = \mathbf{E}_0(7 + 9n, 3 + 3n) = \frac{1}{2}f,
\end{aligned}$$

$$-\mathbf{E}_0(2 + n, 5 + 8n) = \mathbf{E}_0(3 + 2n, 5 + 8n) = f,$$

$$\begin{aligned}
-\mathbf{E}_0(3, 8 + 9n) &= \mathbf{E}_0(3, 6 + 9n) = \mathbf{E}_0(3 + n, 8 + 8n) = -\mathbf{E}_0(3 + n, 6 + 8n) \\
&= \mathbf{E}_0(4 + 2n, 8 + 8n) = \mathbf{E}_0(4 + 2n, 6 + 8n) = \mathbf{E}_0(4 + 3n, 8 + 9n) = \mathbf{E}_0(4 + 3n, 6 + 9n) \\
&= -\mathbf{E}_0(6 + 8n, 3 + n) = \mathbf{E}_0(6 + 8n, 4 + 2n) = \mathbf{E}_0(6 + 9n, 3) = \mathbf{E}_0(6 + 9n, 4 + 3n) = 2f,
\end{aligned}$$

$$-\mathbf{E}_0(7 + 8n, 4 + n) = \mathbf{E}_0(7 + 8n, 5 + 2n) = \mathbf{E}_0(7 + 9n, 4) = \mathbf{E}_0(7 + 9n, 5 + 3n) = \frac{9}{2}f,$$

$$\begin{aligned} -\mathbf{E}_0(1 + j, 6 + 9n + j) &= \mathbf{E}_0(1 + j, 4 + 9n + j) = \mathbf{E}_0(1 + n + j, 6 + 8n + j) \\ &= -\mathbf{E}_0(1 + n + j, 4 + 8n + j) = \mathbf{E}_0(2 + 2n + j, 6 + 8n + j) \\ &= \mathbf{E}_0(2 + 2n + j, 4 + 8n + j) = \mathbf{E}_0(2 + 3n + j, 6 + 9n + j) \\ &= \mathbf{E}_0(2 + 3n + j, 4 + 9n + j) = \frac{1}{2}j^2f, \end{aligned}$$

$$\begin{aligned} -\mathbf{E}_0(5 + 8n + j, 2 + n + j) &= \mathbf{E}_0(5 + 8n + j, 3 + 2n + j) = \mathbf{E}_0(5 + 9n + j, 2 + j) \\ &= \mathbf{E}_0(5 + 9n + j, 3 + 3n + j) = \frac{1}{2}(j + 1)^2f, \end{aligned}$$

$$\begin{aligned} \mathbf{E}_0(5 + 8n + j, n + j) &= \mathbf{E}_0(5 + 8n + j, 1 + 2n + j) = -\mathbf{E}_0(5 + 9n + j, j) \\ &= \mathbf{E}_0(5 + 9n + j, 1 + 3n + j) = \frac{1}{2}(j - 1)^2f, \end{aligned}$$

$$\begin{aligned} \mathbf{E}_0(1 + n, 4 + 10n) &= -\mathbf{E}_0(1 + 2n, 4 + 9n) = \mathbf{E}_0(2 + 3n, 4 + 9n) = \mathbf{E}_0(2 + 4n, 4 + 10n) \\ &= \frac{1}{2}n^2f, \end{aligned}$$

$$\begin{aligned} \mathbf{E}_0(5 + 9n, 2n) &= \mathbf{E}_0(5 + 9n, 1 + 3n) = -\mathbf{E}_0(5 + 10n, n) = \mathbf{E}_0(5 + 10n, 1 + 4n) \\ &= \frac{1}{2}(n - 1)^2f, \end{aligned}$$

$$\begin{aligned} -\mathbf{E}_0(2, 7 + 8n) &= -\mathbf{E}_0(2 + n, 7 + 9n) = -\mathbf{E}_0(3 + 2n, 7 + 9n) = \mathbf{E}_0(3 + 3n, 7 + 8n) \\ &= -\mathbf{E}_0(5 + 8n, 2) = -\mathbf{E}_0(5 + 8n, 3 + 3n) = -\mathbf{E}_0(7 + 8n, 2) = \mathbf{E}_0(7 + 8n, 3 + 3n) \\ &= -\mathbf{E}_0(7 + 9n, 2 + n) = -\mathbf{E}_0(7 + 9n, 3 + 2n) = \frac{1}{2}g_0, \end{aligned}$$

$$-\mathbf{E}_0(2, 5 + 8n) = -\mathbf{E}_0(3 + 3n, 5 + 8n) = g_0,$$

$$\begin{aligned} -\mathbf{E}_0(3, 8 + 8n) &= -\mathbf{E}_0(3, 6 + 8n) = -\mathbf{E}_0(3 + n, 8 + 9n) = -\mathbf{E}_0(3 + n, 6 + 9n) \\ &= -\mathbf{E}_0(4 + 2n, 8 + 9n) = \mathbf{E}_0(4 + 2n, 6 + 9n) = \mathbf{E}_0(4 + 3n, 8 + 8n) = -\mathbf{E}_0(4 + 3n, +8n) \\ &= -\mathbf{E}_0(6 + 8n, 3) = -\mathbf{E}_0(6 + 8n, 4 + 3n) = -\mathbf{E}_0(6 + 9n, 3 + n) = \mathbf{E}_0(6 + 9n, 4 + 2n) \\ &= 2g_0, \end{aligned}$$

$$-\mathbf{E}_0(7 + 8n, 4) = -\mathbf{E}_0(7 + 8n, 5 + 3n) = -\mathbf{E}_0(7 + 9n, 4 + n) = \mathbf{E}_0(7 + 9n, 5 + 2n) = \frac{9}{2}g_0,$$

$$\begin{aligned} -\mathbf{E}_0(1 + j, 6 + 8n + j) &= -\mathbf{E}_0(1 + j, 4 + 8n + j) = -\mathbf{E}_0(1 + n + j, 6 + 9n + j) \\ &= -\mathbf{E}_0(1 + n + j, 4 + 9n + j) = -\mathbf{E}_0(2 + 2n + j, 6 + 9n + j) \\ &= \mathbf{E}_0(2 + 2n + j, 4 + 9n + j) = \mathbf{E}_0(2 + 3n + j, 6 + 8n + j) \\ &= -\mathbf{E}_0(2 + 3n + j, 4 + 8n + j) = \frac{1}{2}j^2g_0, \end{aligned}$$

$$\begin{aligned} -\mathbf{E}_0(5 + 8n + j, 2 + j) &= -\mathbf{E}_0(5 + 8n + j, 3 + 3n + j) = -\mathbf{E}_0(5 + 9n + j, 2 + n + j) \\ &= \mathbf{E}_0(5 + 9n + j, 3 + 2n + j) = \frac{1}{2}(j + 1)^2g_0, \end{aligned}$$

$$\begin{aligned}
-\mathbf{E}_0(5 + 8n + j, j) &= \mathbf{E}_0(5 + 8n + j, 1 + 3n + j) = -\mathbf{E}_0(5 + 9n + j, n + j) \\
&= -\mathbf{E}_0(5 + 9n + j, 1 + 2n + j) = \frac{1}{2}(j - 1)^2 g_0, -\mathbf{E}_0(1 + n, 4 + 9n) \\
&= -\mathbf{E}_0(1 + 2n, 4 + 10n) = \mathbf{E}_0(2 + 3n, 4 + 10n) = -\mathbf{E}_0(2 + 4n, 4 + 9n) \\
&= \frac{1}{2}n^2 g_0, \\
-\mathbf{E}_0(5 + 9n, n) &= \mathbf{E}_0(5 + 9n, 1 + 4n) = -\mathbf{E}_0(5 + 10n, 2n) = -\mathbf{E}_0(5 + 10n, 1 + 3n) \\
&= \frac{1}{2}(n - 1)^2 g_0,
\end{aligned}$$

where

$$\begin{aligned}
a &= EI^s, \quad b = \rho I^s \Omega^2, \quad c = \rho A \Omega^2, \quad d = \rho I_p^s \Omega^2, \\
f &= \rho A e_u^s \Omega^2, \quad g_0 = \rho A e_v^s \Omega^2, \quad h = GI_p^s, \quad m = k_s AG, \quad s = \rho \Omega^2 A (e^s)^2 + \rho \Omega^2 I_p^s, \\
i &= 1, 2, 3, \dots, n, \quad \text{and } j = 3, 4, 5, \dots, n - 1.
\end{aligned}$$

References

- [1] F.F. Ehrich, *Handbook of Rotordynamics*, McGraw-Hill, New York, 1992.
- [2] R.L. Ruhl, J.F. Booker, A finite element model for distributed parameter turborotor systems, *Journal of Engineering for Industry* 94 (1972) 126–132.
- [3] H.D. Nelson, J.M. McVaugh, The dynamics of rotor-bearing systems using finite elements, *Journal of Engineering for Industry* 98 (1976) 593–600.
- [4] H.D. Nelson, A finite rotating shaft element using timoshenko beam theory, *Journal of Mechanical Design* 102 (1980) 793–803.
- [5] N.H. Özgüven, L.Z. Özkan, Whirl speeds and unbalance response of multibearing rotors using finite elements, *Journal of Vibration, Stress, and Reliability in Design* 106 (1984) 72–79.
- [6] G. Genta, Whirling of unsymmetrical rotors: a finite element approach based on complex co-ordinates, *Journal of Sound and Vibration* 124 (1988) 27–53.
- [7] Y. Kang, Y.P. Shih, A.C. Lee, Investigation on the steady-state responses of asymmetric rotors, *Journal of Vibration and Acoustics* 114 (1992) 194–208.
- [8] A.C. Lee, Y. Kang, K.L. Tsai, K.M. Hsiao, Transient analysis of an asymmetric rotor-bearing system during acceleration, *Journal of Engineering for Industry* 114 (1992) 465–475.
- [9] M.A. Prohl, A general method for calculating critical speeds of flexible rotors, *Journal of Applied Mechanics* 12 (1945) 142–148.
- [10] E.C. Koenig, Analysis for calculating lateral vibration characteristics of rotating systems with any number of flexible supports Part 1—the method of analysis, *Journal of Applied Mechanics* 28 (1961) 585–590.
- [11] T.G. Guenther, D.C. Lovejoy, Analysis for calculating lateral vibration characteristics of rotating systems with any number of flexible supports Part 2—application of the method of analysis, *Journal of Applied Mechanics* 28 (1961) 591–600.
- [12] J.W. Lund, Stability and damped critical speeds of a flexible rotor in fluid-film bearings, *Journal of Engineering for Industry* 96 (1974) 509–517.
- [13] P.N. Bansal, R.G. Kirk, Stability and damped critical speeds of rotor-bearing systems, *Journal of Engineering for Industry* 97 (1975) 1325–1332.
- [14] J.W. Lund, Sensitivity of the critical speeds of a rotor to changes in the design, *Journal of Mechanical Design* 102 (1980) 115–121.

- [15] K.B. Yim, S.T. Noah, J.M. Vance, Effect of tangential torque on the dynamics of flexible rotors, *Journal of Applied Mechanics* 53 (1986) 711–718.
- [16] J.W. Lund, F.K. Orcutt, Calculations and experiments on the unbalance response of a flexible rotor, *Journal of Engineering for Industry* 89 (1967) 785–796.
- [17] T. Inagaki, H. Kanki, K. Shiraki, Response analysis of a general asymmetric rotor-bearing system, *Journal of Mechanical Design* 102 (1980) 147–157.
- [18] J.W. David, L.D. Mitchell, J.W. Daws, Using transfer matrices for parametric system forced response, *Journal of Vibration, Acoustics, Stress, and Reliability in Design* 109 (1987) 356–360.
- [19] A.C. Lee, Y. Kang, S.L. Liu, A modified transfer matrix method for linear rotor-bearing systems, *Journal of Applied Mechanics* 58 (1991) 776–783.
- [20] A.C. Lee, Y.P. Shih, Y. Kang, The analysis of linear rotor-bearing systems: a general transfer matrix method, *Journal of Vibration and Acoustics* 115 (1993) 490–496.
- [21] Y. Kang, A.C. Lee, Y.P. Shih, A modified transfer matrix method for asymmetric rotor-bearing systems, *Journal of Vibration and Acoustics* 116 (1994) 309–317.
- [22] E.C. Pestel, F.A. Leckie, *Matrix Methods in Elastomechanics*, McGraw-Hill, New York, 1963.
- [23] W.D. Pilkey, P.Y. Chang, *Modern Formulas for Statics and Dynamics: A Stress-and-Strain Approach*, McGraw-Hill, New York, 1978.
- [24] S. Sankar, On the torsional vibration of branched systems using extended transfer matrix method, *Journal of Mechanical Design* 101 (1979) 546–553.
- [25] J.S. Rao, *Rotor Dynamics*, Wiley Eastern, New Delhi, 1991.
- [26] P. Schwibinger, R. Nordmann, The influence of torsional–lateral coupling on the stability behavior of geared rotor systems, *Journal of Engineering for Gas Turbines and Power* 110 (1988) 563–571.
- [27] Q.H. Qin, C.X. Mao, Coupled torsional–flexural vibration of shaft systems in mechanical engineering—I: finite element model, *Computers and Structures* 58 (1996) 835–843.
- [28] J.S. Rao, T.N. Shiau, J.R. Chang, Theoretical analysis of lateral response due to torsional excitation of geared rotors, *Mechanism and Machine Theory* 33 (1998) 761–783.
- [29] M.A. Mohiuddin, Y.A. Khulief, Coupled bending torsional vibration of rotors using finite element, *Journal of Sound and Vibration* 223 (1999) 297–316.
- [30] B.O. Al-Bedoor, Dynamic model of coupled shaft torsional and blade bending deformations in rotors, *Computer Methods in Applied Mechanics and Engineering* 169 (1999) 177–190.
- [31] B.O. Al-Bedoor, Modeling the coupled torsional and lateral vibrations of unbalanced rotors, *Computer Methods in Applied Mechanics and Engineering* 190 (2001) 5999–6008.
- [32] C.W. Lee, *Vibration Analysis of Rotor*, Kluwer Academic Publishers, London, 1993.
- [33] L.M. Greenhill, W.B. Bickford, H.D. Nelson, A conical beam finite element for rotor dynamics analysis, *Journal of Vibration, Acoustics, Stress, and Reliability in Design* 107 (1985) 421–430.
- [34] C. Hayashi, *Nonlinear Oscillations in Physical Systems*, McGraw-Hill, New York, 1964.